C1. Kinetics and Mechanism for the Reaction of $C_6H_5C_2H_2$ with O_2: A Computational and Experimental Study

***J. Park*, Y. M. Choi, L. Wang and M. C. Lin**

Emory University, Department of Chemistry, 1515 Dickey Drive, Atlanta, GA, 30322
jpark05@emory.edu, yongman.choi@mse.gatech.edu, liming@chemistry.leeds.ac.uk, mclin@emory.edu

The effects of temperature and pressure on the formation and decomposition of $C_6H_5C_2H_2O_2$ in the $C_6H_5C_2H_2 + O_2$ reaction have been investigated at temperatures from 298 - 358 K by directly monitoring the $C_6H_5C_2H_2O_2$ radical in the visible region with cavity ringdown spectrometry. The rate constants for the $C_6H_5C_2H_2 + O_2$ association and for the fragmentation of $C_6H_5C_2H_2O_2$ were respectively found to be

$$k_1 = (2.84 \pm 1.21) \times 10^{11} \exp(+780/T)\ cm^3\ mol^{-1}\ s^{-1}$$
$$k_2 = (1.68 \pm 0.10) \times 10^4\ s^{-1}.$$

k_1 was found to be weakly dependent on pressure in the range of 40-150 Torr Ar, whereas k_2 was found to be independent of pressure. The mechanism for this very fast reaction has been elucidated quantum-chemically by B3LYP/6-31G+(d,p) calculations. The result of the calculations indicated that the reaction effectively occur by two competitive association paths giving 3- and 4-member-ring peroxide intermediates which fragment rapidly to C_6H_5CHO + CHO with a predicted 91.4 kcal/mol exothermicity. A full RRKM calculation on the system is underway.

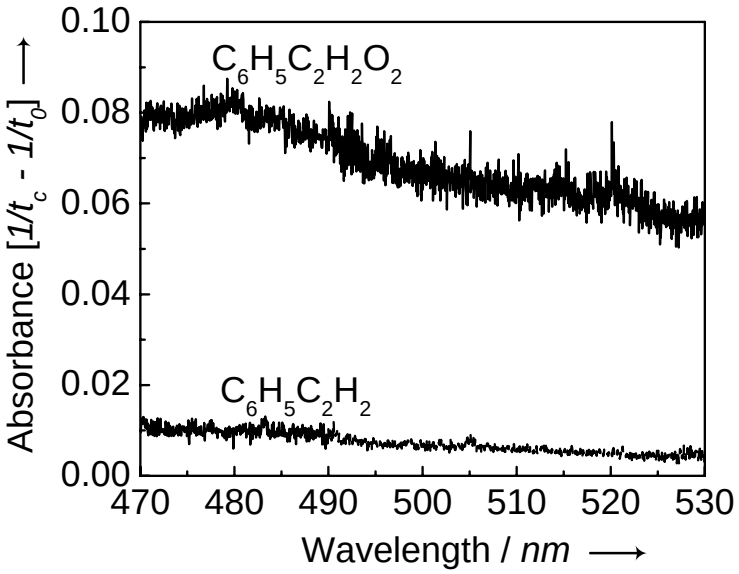

Figure 1. Absorption spectra of $C_6H_5C_2H_2$ and $C_6H_5C_2H_2O_2$ detected by CRDS at 100 μs after the photolysis of 0.1 % of β-bromostyrene at 248 nm in Ar without and with added O_2.

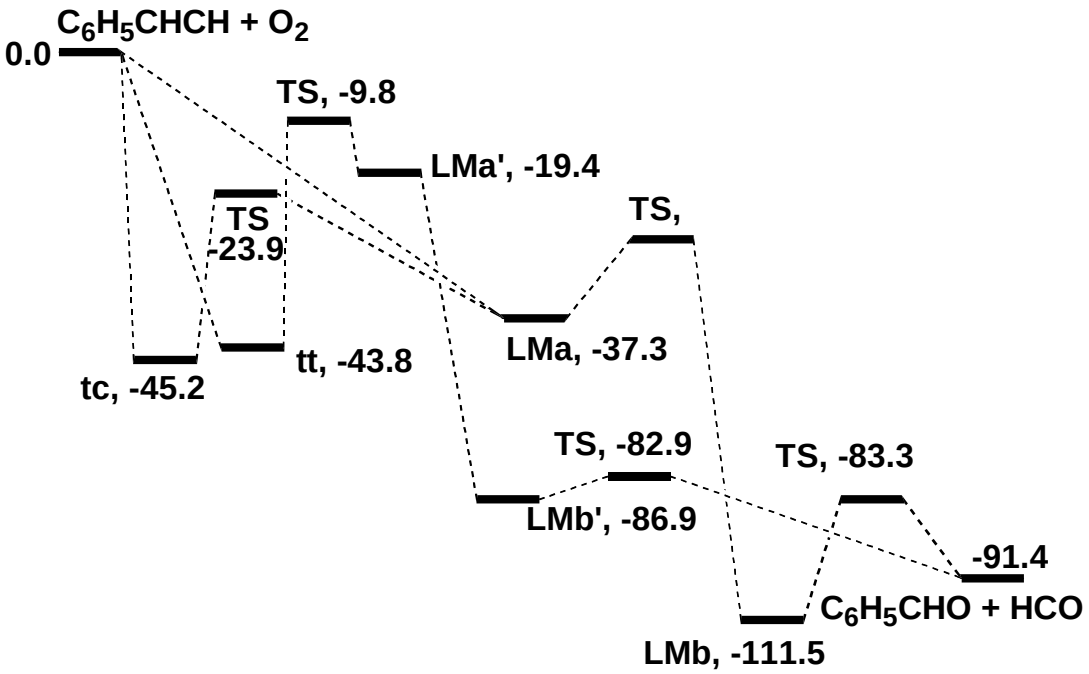

Figure 2. The PES for the reaction of $C_6H_5C_2H_2$ +O_2 computed at the B3LYP/6-31+G(d) levels. Energies are in kcal/mol; *tt*- and *tc*-isomer represent *trans, trans*- and *trans, cis*-isomer, respectively.

C2. Isomerization and Decomposition of C_3H_3I

***R. Sivaramakrishnan*[a], *W. Tang*[b], *R. S. Tranter*[c] *and K. Brezinsky**[d]

a. Department of Mechanical & Industrial Engineering, University of Illinois at Chicago, 2039, Engineering Research Facility, 842, W. Taylor Street, Chicago, Il-60607.
Email: rsivar1@uic.edu
b. Department of Chemical Engineering, University of Illinois at Chicago, 810, South Clinton Street, Chicago, Il-60607.
Email: wtang4@uic.edu
c. Chemistry Division, Argonne National Laboratory, Argonne, Il-60439.
Email: tranter@anl.gov
d. Department of Mechanical & Industrial Engineering, University of Illinois at Chicago, 2039, Engineering Research Facility, 842, W. Taylor Street, Chicago, Il-60607.
Email: kenbrez@uic.edu

Precursor soot chemistry has been one of the primary thrust areas within the combustion chemistry community over the past few years. There have been a number of experimental and theoretical studies on precursor soot chemistry involving the recombination of propargyl radicals (C_3H_3) [A summary of prior studies can be found in a recent publication from our laboratory-Ref 1] which is thought to be one of the dominant routes for the formation of the first aromatic ring, benzene.

In a large majority of the experimental studies the propargyl halides C_3H_3X (X=Cl, Br, I) were used as the source for the C_3H_3 radical. Recently experiments have been performed in the UIC High Pressure Single Pulse Shock tube using C_3H_3I as a source for the C_3H_3 radical [1]. Propargyl iodide (P-C_3H_3I) was synthesized from propargyl bromide using the Finkelstein reaction. As much as 5% of the isomeric form, allenyl iodide (A-C_3H_3I) was detected in the synthesized reagent mixtures.

The synthesized C_3H_3I was used to perform experiments over the temperature range from 600-1300 K at post-shock pressures of 50 bars. GC/FID-TCD and GC/MS were the analytical technique used in these experiments. Of interest to the present study are the experiments performed at lower temperatures from 600 K to around 800 K. Figure 1 depicts the ratio of A-C_3H_3I to P-C_3H_3I as a function of temperature. Below 600K no reaction is observed. As the temperature is increased above 600 K, the propargyl iodide isomerizes to allenyl iodide with the relative ratio of allenyl iodide being as high as 0.9 at 750 K. No other species was formed/detected in this temperature range and the carbon recovery was complete over this temperature range. Dissociation of the C_3H_3I begins to compete with the isomerization at temperatures>700 K and becomes dominant at temperatures beyond 750K with the relative ratio of A-C_3H_3I dropping at higher temperatures. Furthermore the recombination products of C_3H_3 (propargyl) begin to appear (initial products are the three linear C_6H_6 species 1, 5 Hexadiyne, 1, 3 Hexadien-5-yne, 3, 4-dimethylenecyclobutene, See Ref. 2). The observed intermediates in these studies are consistent with prior studies in our laboratory on the pyrolysis of 1, 5-Hexadiyne [2].

The observation of isomerization seems to be surprising given the fairly low C-I bond dissociation energies (BDE) ~ 42-45 kcal/mol (0 K) for the C_3H_3I isomers. Isomerization has

been observed to occur in the smaller halides, C_3H_3F and C_3H_3Cl. Ab-initio studies on C_3H_3X isomerization are scarce and are primarily based on the study by Honjou [3] who was able to explain the isomerization of C_3H_3F via a cyclic intermediate. The surface is similar to the C_3H_4 surface which has been studied in great detail with recent studies involving very high level calculations in a recent study by Miller and Klippenstein [4]. By analogy with the C_3H_4 and C_3H_3F surfaces isomerization in C_3H_3Cl [5] was also explained using a cyclic intermediate though the intermediate was not observed/detected in those experiments. By analogy Kern et al. [6] have also utilized the C_3H_4 surface to explain isomerization in C_3H_3Br. However the C-Br BDE in propargyl bromide is ~60 Kcal/mol and at low temperatures one might expect to observe isomerization.

To investigate the possible mechanistic routes for the isomerization to occur we have performed electronic structure calculations using the Gaussian 98 [7] suite of programs. The results of our ab-initio calculations shown in Figure 2 indicate that the isomerization of P-C_3H_3I to A-C_3H_3I does not proceed in an analogous manner to the lower C_3H_3X (X=H, F, Cl, Br) homologues. The barriers involved in isomerizing to the intermediate cyclic structure via H atom transfer are far too high. Consequently it is questionable that the cyclic structure is formed (even if formed it would be present in very low concentrations) and in the present experiments too the cyclic species was not detected. Energies for other feasible C_3H_3I intermediates (CH_2CHI, c-CH_2CHI) all lie above the critical energies for C_3H_3+I. Taking into account the low C-I bond dissociation energies the isomerization at low temperatures can be reconciled at present via a simple sequence of reactions (shown below) involving the dissociation of C_3H_3I and the

P-C_3H_3I= C_3H_3+I
C_3H_3+I= P-C_3H_3I
A-C_3H_3I= C_3H_3+I
C_3H_3+I= A-C_3H_3I
I+I=I_2

subsequent recombination of the C_3H_3 and I. Furthermore a brief survey in the NIST chemical kinetics database reveals only 2 reported measurements of second order recombination rates for I+I=I_2 with the only direct study being that by Hippler et al. [8]. They studied the recombination of I atoms at high pressures from 0.1-100 bars at 314K and their reported rates lie between 1E+13 - 7E+13. The possibility of I+I competing with C_3H_3+I cannot be ruled out under the experimental conditions of the present set of experiments.

Given the lack of experimental studies on C_3H_3I dissociation we have also performed electronic structure calculations to obtain accurate estimates of BDE's as well as map out the bond dissociation profile in P-C_3H_3I and A-C_3H_3I. The energetics from these calculations were used in conjunction with Canonical Variational Transition State Theory (CVTST) to extract rate parameters for the C-I dissociation in P-C_3H_3I and A-C_3H_3I. The experimental data and the predictions made by the proposed mechanism will be presented.

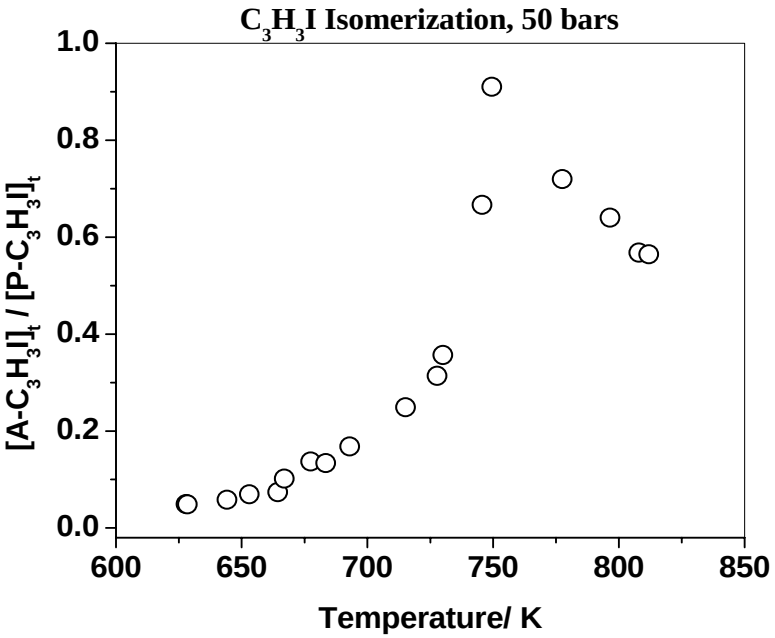

Figure 1: Single pulse shock tube data, 50 bars

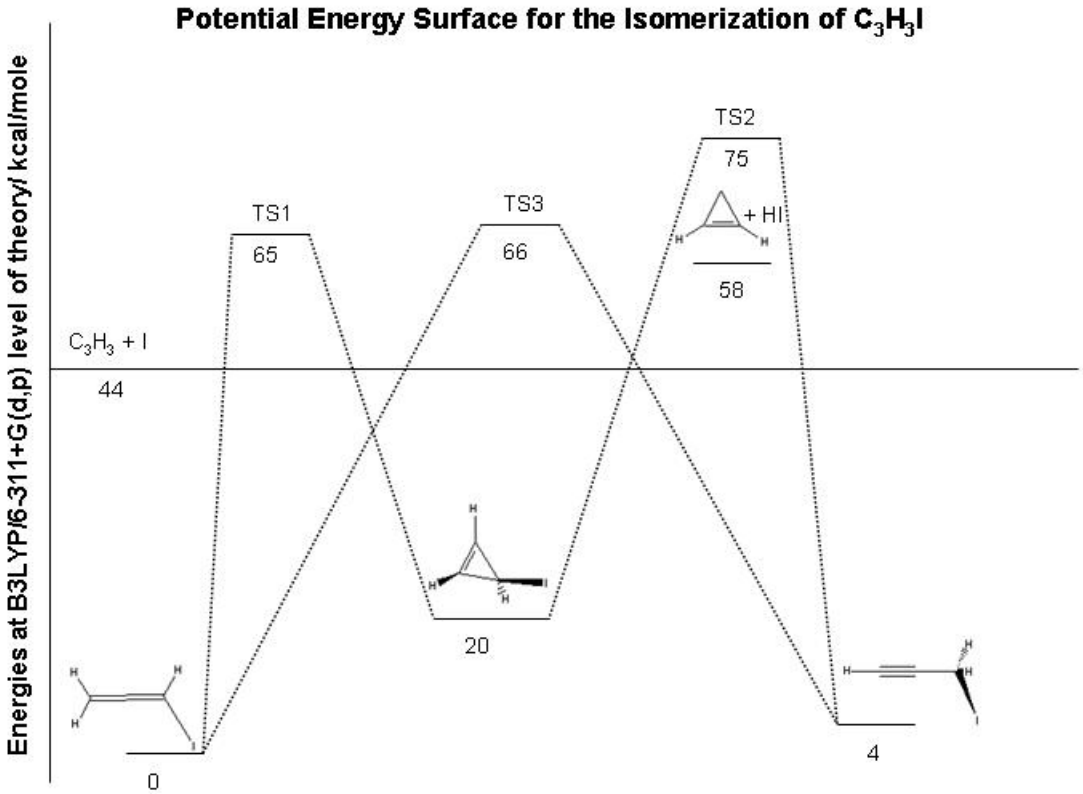

Figure 2: Singlet surface at B3LYP/6-311+G(d, p) level of theory

Acknowledgements

The authors gratefully acknowledge financial support for this research from the U. S. Department of Energy, Office of Basic Energy Sciences, Chemical Sciences Division through grant # DE-FG0298ER14897 and the National Science Foundation through contract CTS 0109053. Support for R. S. Tranter was provided under the auspices of the Office of Basic Energy Sciences, Division of Chemical Sciences, Geosciences and Biosciences, U. S. Department of Energy, under contract number W-31-109-ENG-38. We thank Prof. J. H. Kiefer at the University of Illinois at Chicago for providing insightful comments and advice.

References

1. Tang, W.; Tranter, R. S.; Brezinsky, K. J. Phys. Chem. A In Press, 2005
2. Tranter, R. S.; Tang, W.; Anderson, K. B.; Brezinsky, K. J. Phys. Chem. A 2004 108, 3406-3415.
3. Honjou, N. J. Phys. Chem. 1988 92, 2410-2415.
4. Miller, J. A.; Klippenstein, S. J. J. Phys. Chem. A 2003 107, 2680-2692.
5. Kumaran, S. S.; Lim, K. P. ; Michael, J. V.; Tilson, J. L.; Suslensky, A.; Lifshitz, A. Israel Journal of Chemistry 1996 36, 223-232.
6. Kern, R. D.; Chen, H.; Kiefer, J. H.; Mudipalli, P. S. Combustion and Flame, 1995 100, 177-184.
7. Frisch, M. J.; Trucks, G. W.; Schlegel, H. B.; Scuseria, G. E.; Robb, M. A.; Cheeseman, J. R.; Zakrzewski, V. G.; Montgomery, J. A. Jr.; Stratmann, R. E.; Burant, J. C.; Dapprich, S.; Millam, J. M.; Daniels, A. D.; Kudin, K. N.; Strain, M. C.; Farkas, O.; Tomasi, J.; Barone, V.; Cossi, M.; Cammi, R.; Mennucci, B.; Pomelli, C.; Adamo, C.; Clifford, S.; Ochterski, J.; Petersson, G. A.; Ayala, P. Y.; Cui, Q.; Morokuma, K.; Rega, N.; Salvador, P.; Dannenberg, J. J.; Malick, D. K.; Rabuck, D.; Raghavachari, K.; Foresman, J. B.; Cioslowski, J.; Ortiz, J. V.; Baboul, A. G.; Stefanov, B. B.; Liu, G.; Liashenko, A.; Piskorz, P.; Komaromi, I.; Gomperts, R.; Martin, R. L.; Fox, D. J.; Keith, T.; Al-Laham, M. A.; Peng, C. Y.; Nanayakkara, A.; Challacombe, M.; Gill, P. M. W.; Johnson, B.; Chen, W.; Wong, M. W.; Andres, J. L.; Gonzalez, C.; Head-Gordon, M.; Replogle, E. S.; Pople, J. A. *Gaussian 98*, Revision A.11.3, Gaussian, Inc., Pittsburgh PA, 2002.
8. Hippler, H.; Luther, K.; Troe, J. Ber. Bunsenges. Phys. Chem. 1973 77, 1104-1114.

C3. *Ab Initio* Study on the Termolecular Reaction of 2NO + O_2 and the Complex Self-Reaction of NO_2

Y. M. Choi[a,b], ***M. C. Lin***[a]

[a] Department of Chemistry, Emory University, 1515 Dickey Drive, Atlanta, GA 30322, USA
E-mail: chemmcl@emory.edu
[b] present address: School of Materials Science & Engineering, Georgia Institute of Technology, 771 Ferst Drive, N.W., Atlanta, GA 30332, USA
E-mail: yongman.choi@mse.gatech.edu

Reaction mechanisms for the termolecuar reaction of NO with O_2, as well as that for the self-reaction of NO_2 have been elucidated by various quantum-chemical methods. The G2M(CC)//G96LYP/6-31+G(d) composite method was applied to evaluate the accurate energetics and construct the potential energy surfaces after examining the reliability of the computed thermochemical data based on available experimental and theoretical values. The kinetics of the termolecular 2NO + O_2 reaction have been theoretically predicted for the first time to account for its weak negative T-dependence since Gershinowitz and Eyring (*J. Am. Chem. Soc.* **1935**, *57*, 985) interpreted the experimental data. The barrierless pathways forming *cis,cis*-ONOONO, O_2NNO_2, and *trans*-$ONONO_2$ shown in Fig. 1 have been mapped out following their minimum energy paths and the corresponding rate constants were evaluated with a canonical variational approach by RRKM/ME calculations or by the flexible transition-state theory.

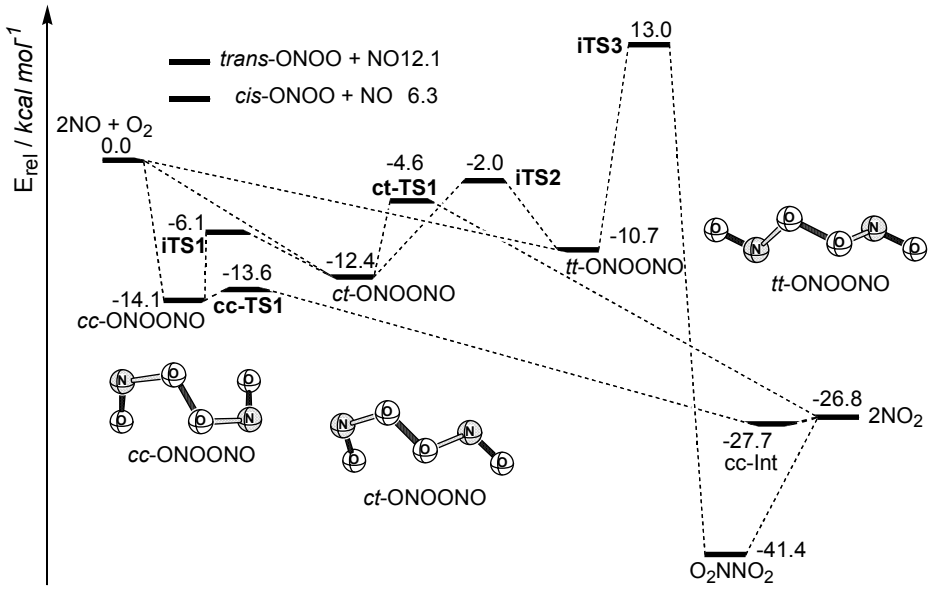

Fig. 1. Schematic energy profiles for the termolecular reaction of 2NO + O_2 → $2NO_2$ computed at the G2M(CC)//G96LYP/6-31+G(d). *cc*-, *ct*- and *tt*- represent *cis,cis*-, *cis,trans*- and *trans, trans*-, respectively.

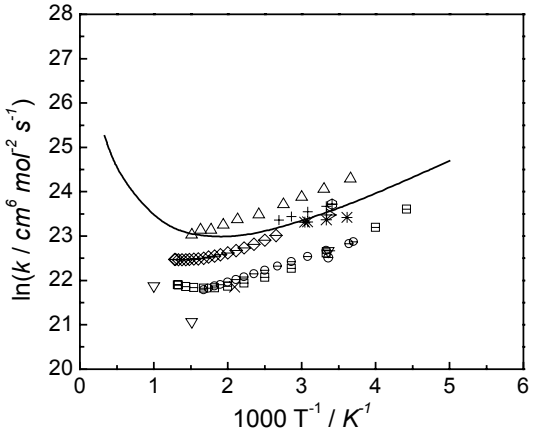

Fig 2. Total rate constants for the termolecular reaction of $2NO + O_2 \rightarrow 2NO_2$. Solid curve represents the predicted values.

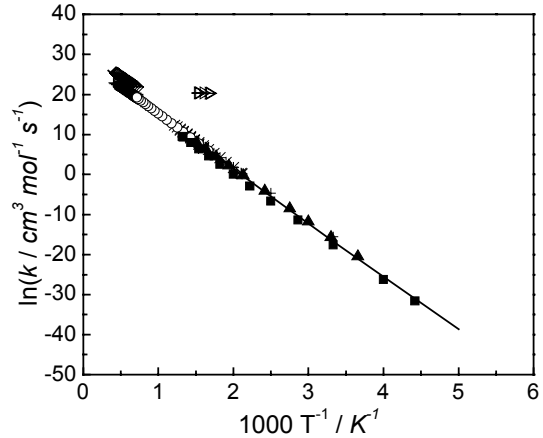

Fig 3. Comparison of experimental and predicted rate constants for the bimolecular reaction of $2NO_2 \rightarrow 2NO + O_2$. Solid symbols, (■) and (▲), are derived from the forward termolecular reaction of $2NO + O_2 \rightarrow 2NO_2$ according to the expression $k_{-1} = k_1/K_{eq,1}$. Solid line corresponds to the predicted values.

For practical applications, as depicted in Figs 2 and 3, the rate constants evaluated for the atmospheric-pressure or high-pressure condition can be represented by modified Arrhenius equations for the temperature range of 200 – 3000 K: $k_1 = 2.6 \times 10^2\ T^{2.4} \exp(1300/T)$ cm^6 mol^{-2} s^{-1}, $k_2^{\infty} = 6.8 \times 10^{21}\ T^{-2.0} \exp(-6990/T)$ s^{-1} and $k_3 = 2.0\times10^8\ T^{1.3} \exp(-11400/T)$ cm^3 mol^{-1} s^{-1}, where **1**, **2**, and **3** represent the reactions of $2NO + O_2 \rightarrow 2NO_2$, $O_2NNO_2 \rightarrow 2NO_2$, and $2NO_2 \rightarrow NO_3 + NO$, respectively. In addition, we estimated their reverse rate constants, $k_{-1} = 8.4 \times 10^7\ T^{1.5} \exp(-13000/T)$, $k_{-2}^{\infty} = 1.6 \times 10^{17}\ T^{-2.1} \exp(-70/T)$ and $k_{-3} = 2.5\times10^{11}\ T^{0.5} \exp(360/T)$ cm^3 mol^{-1} s^{-1}, which are in very good agreement with available experimental data.

Acknowledgments:
We thank the Cherry L. Emerson Center of Emory University for the use of its resources, which are in part supported by a National Science Foundation grant (CHE-0079627) and an IBM shared University Research Award. YMC sincerely acknowledges the Office of Naval Research under contract no. N00014-89-J1949, Dr. J. Goldwasser program manager, for financial support. MCL acknowledges the support from Taiwan National Science Council for a Distinguished Visiting Professorship at the Center for Interdisciplinary Molecular Science, Chiao Tung University, Hsinchu, Taiwan.

C4. Reaction Paths, Kinetics and Thermochemical Properties on Reaction of Methylthiyl (CH_3S) and Methylthiomethyl (CH_3SCH_2) Radicals with O_2

Li Zhu, Fei Jin and Joseph W. Bozzelli*

Department of Chemistry, *New Jersey Institute of Technology,*
University Heights, Newark, NJ 07102, USA
Bozzelli@adm.njit.edu, Tel. 973-896-3459

The $CH_3S\bullet + O_2$ reaction system is important system for both combustion and atmospheric chemistry in understanding kinetics of the exothermic conversion of thiol radicals (methylthiyl, $CH_3S\bullet$) in the atmosphere. It also serves as a surrogate reaction for estimation of longer chain and substituted thiol radical reactions with molecular oxygen.

$CH_3S\bullet + {}^3O_2$ with possible ultimate products $CH_3 + SO_2$ $\Delta H_{rxn,298} = -66.0$ kcal/mol.

We review the experimental and computational chemistry literature on the $CH_3S\cdot + O_2$ reaction system and use computational chemistry to further evaluate thermochemistry and a number of reaction paths and barriers along with the enthalpies of formation for stable intermediates. Enthalpies of formation for products and radical intermediates are computed by isodesmic work reactions at the CBS-QB3 level of theory. Barriers for important reaction paths from B3LYP/6-311++G(d,p), B3LYP/6-311++G(3df,2p), CCSD(T)/6-311G(d,p)//MP2/6-31G(d,p), B3P86/6-311G(2d,2p)//B3P86/6-31G(d), B3PW91/6-311++G(3df,2p), G3MP2, and CBS-QB3 are compared. Results are shown to depend on the calculation levels and basis set. Enthalpy values from the G3MP2 and CBS-QB3 composite methods are recommended for these carbon – sulfur – oxygen systems, when feasible. Intramolecular rotation potentials are calculated at the B3LYP/6-31G(d,p) level and used to determine contributions to entropy and heat capacities. The well depth for the $CH_3S\cdot + {}^3O_2$ reaction to $CH_3SOO\cdot$ adduct is found to be 9.7 kcal/mol. One low barrier outlet channel, $CH_3SOO\cdot \rightarrow CH_2S + HO_2$, is found to have 9.9 (or 13.1) kcal/mol activation energy, relative to the stabilized $CH_3SOO\cdot$ adduct at G3MP2 (CBS-QB3) levels; but has a tight transition state structure relative to reverse reaction. Kinetics parameters are evaluated using chemical activation analysis and unimolecular dissociation of the stabilized adducts.

The potential energy diagram for $CH_3S\bullet$ with ${}^3O_2$ is shown in Figure 1, and our calculations show a shallow well for the $CH_3SOO\bullet$ adduct of 9.7 kcal/mol, in good agreement with prior calculations and experiments. Barriers for two forward reactions, TS6 and TS2', are 9.9 and 24.7 kcal/mol, (relative to the CH_3SOO adduct) respectively. We find TS6 has a lower barrier the abstraction path (TS1), which also results in the $CH_2S + HO_2$ product set.

QRRK calculations for $k(E)$ and master equation analysis for fall-off are performed on $CH_3S\cdot + O_2$ and $CH_3SC\cdot H_2 + O_2$ reaction systems and rate constant versus temperature and pressure are illustrated in Figures 3 to 5.

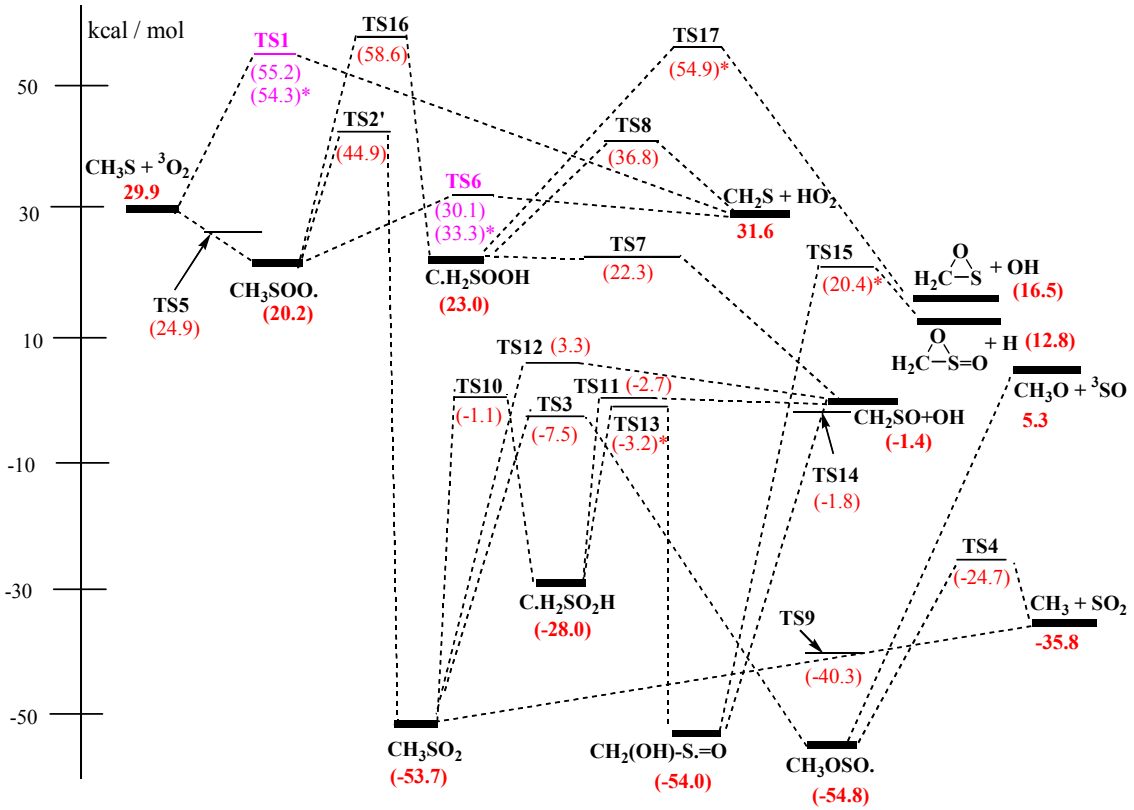

Figure 1: Potential energy diagram at 298 K (in kcal/mol). All barriers are calculated at G3MP2 level except those labeled with * are calculated at CBS-QB3 level.

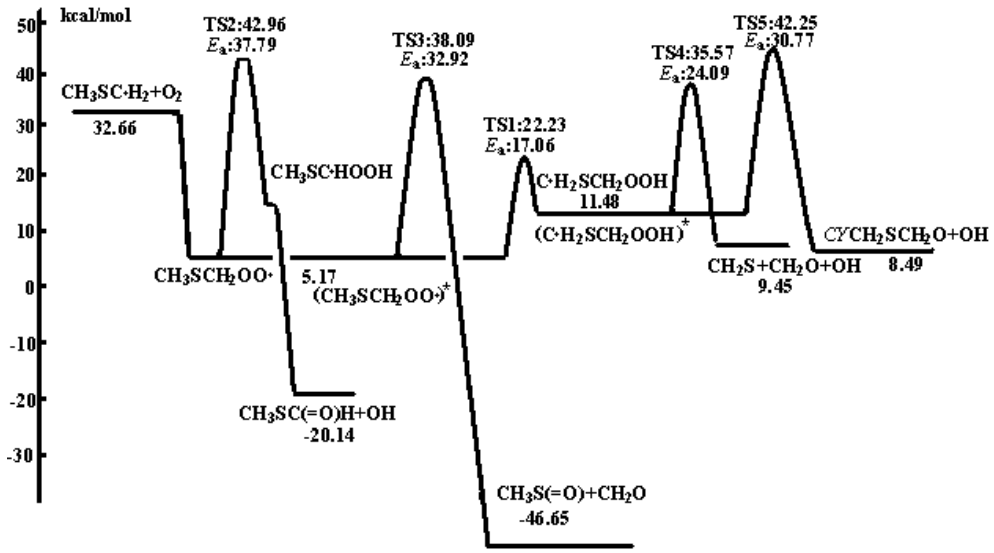

Figure 2: Potential energy diagram of $CH_3SC.H_2 + O_2$ at 298 K (in kcal/mol) at CBS-QB3 level.

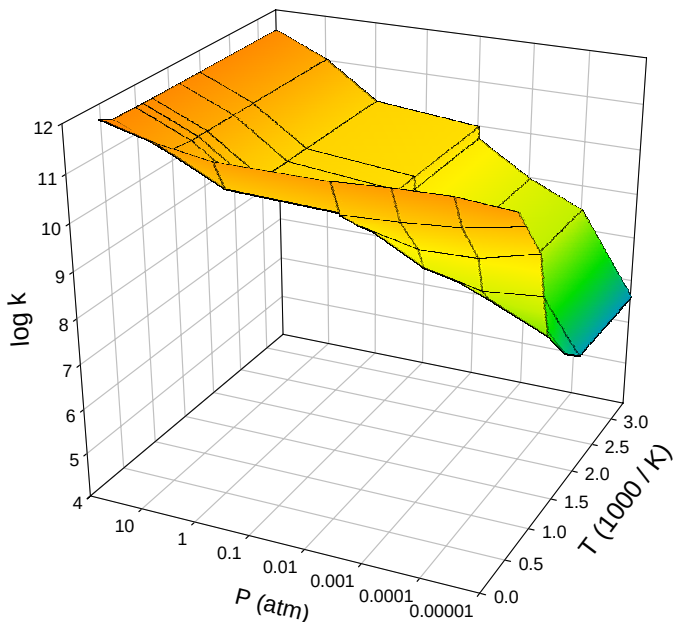

Figure 3: Total forward rate constant of $CH_3S + O_2$ (in cm^3/mol-s).

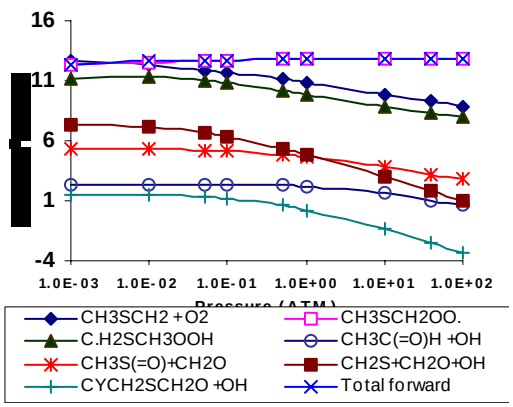

Figure 4: $CH_3SC{\cdot}H_2 + O_2 \rightarrow$ Products log *k* vs. pressure at 298K.

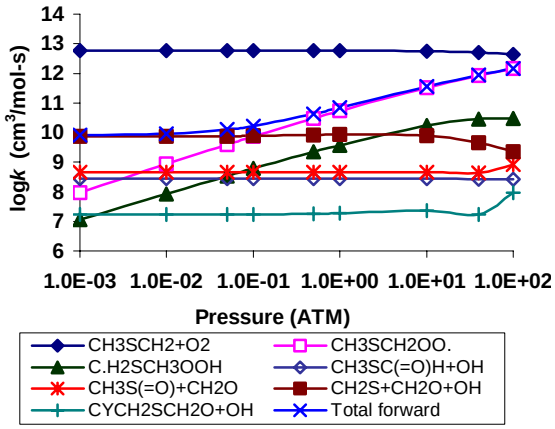

Figure 5: $CH_3SC{\cdot}H_2 + O_2 \rightarrow$ Products log *k* vs. pressure at 1000K.

C5. First-Principles Simulations of the OMCVD of InN on TiO_2 Nanoparticles

***Jeng-Han Wang* and M. C. Lin**

Department of Chemistry, Emory University, Atlanta, GA 30322, USA

We present the results of a computational and experimental study on the adsorption and reactions of the precursors employed in the OMCVD (organometallic chemical vapor deposition) of indium nitride, hydrazoic acid (HN_3) and trimethyl indium ($In(CH_3)_3$), on 15-20 nm TiO_2 nanoparticle films [1]. Experimentally, FTIR spectra of the precursors have been measured by varying their dosages, UV irradiation time and surface annealing temperature. Computationally, molecular structures, vibrational frequencies and adsorption energies of possible adsorbates including HN_3, $In(CH_3)_3$ and their derivatitves, N_3, N_2, NH, H, $In(CH_3)_2$, $In(CH_3)$, In and CH_3, have been predicted by first-principles calculations using the density functional theory (DFT) and the pseudopotential method [2]. The potential energy diagrams for the formation of various absorbates with their transition states have also been established for both systems (see attached figures).

On the basis of HN_3/TiO_2 experimental and computational results, the peak appeared at 2075 cm^{-1}, which increases at a faster rate with HN_3 exposure time, corresponds to the stable adsorbate, N_3-Ti(a), with the predicted adsorption energy, E_{ads} = 13 kcal/mol. The peak at 2118 cm^{-1}, which survives at the highest surface temperature in the heating experiment, is attributable to the most stable adsorbate, Ti-N_2N(H)-O(a) with E_{ads} = 36 kcal/mol. The peak at 2170 cm^{-1}, which vanishes most readily in all of the aforementioned experiments, is related to less stable molecular adsorbates, end-on HN_3-Ti(a) with E_{ads} = 5 kcal/mol and side-on $HN(N_2)$-Ti(a) with E_{ads} = 8 kcal/mol.

On the basis of $In(CH_3)_3/TiO_2$ experimental and computational results, the two sharpest peaks at 2979 and 2925 cm^{-1} detected in the dosage are attributed to the asymmetrical and symmetrical C-H vibrations of methyl groups in $In(CH_3)_3$(a) and its derivatives, $(H_3C)_2$In(a), H_3CIn(a), H_3C(a). In the UV irradiation experiment, the methyl group was quickly oxidized to the methoxy with the C-H vibrations at 2925 and 2822 cm^{-1} and further oxidized to the carboxyl group with vibrations at 2888 cm^{-1} (ν_s(CH)), 1577 cm^{-1} (ν_a(OCO)), 1380 cm^{-1} (δ(CH)) and 1355 cm^{-1} (ν_s(OCO)). Finally, from the computed energies with vibrational analysis, the carboxyl group was confirmed to adsorb on the TiO_2 surface with two oxygen atoms doubly attached to two Ti atoms.

References:

[1]. J. H. Wang and M. C. Lin, ChemPhysChem, 5, 1615-18 (2004).
[2]. Kresse, G.; Hafner, J. *Phys. Rev. B* **1993**, *47*, 558.

C6. On the Chaperon Mechanism in the Reaction ClO + ClO (+M) → Products

***Jing-Yao Liu*[a,b] *and John R. Barker*[a]**

a. Department of Atmospheric, Oceanic, and Space Sciences, University of Michigan, Ann Arbor, Michigan 48109-2143; Email: jrbarker@umich.edu
b. Permanent address: Institute of Theoretical Chemistry, State Key Laboratory of Theoretical and Computational Chemistry, Jilin University, Changchun 130023, P. R. China; Email: jingyao@umich.edu

Chlorine monoxide (ClO) radicals play an important role in the chemistry of the global stratosphere and in polar stratospheric ozone layer depletion. The ClO radical self-reactions have attracted considerable attention experimentally and theoretically because of the key role of the ClO dimer in the formation of the "ozone hole", [1,2]

$$ClO + ClO\ (+M) \rightarrow ClOOCl\ (+M) \qquad (1)$$

where M is the third body. For such three-body reactions, there are two principal reaction mechanisms: the energy transfer mechanism and the chaperone mechanism.

In the energy transfer mechanism, a long-lived vibrationally excited complex is first formed, and then stabilized by energy transfer.

$$ClO + ClO \Leftrightarrow ClOOCl^{**} \qquad (2,-2)$$

$$ClOOCl^{**} + M \rightarrow ClOOCl + M \qquad (3)$$

where the double asterisk denotes vibrational energy in excess of the reaction barrier. In the chaperon mechanism, the reversible Reaction (4) produces a weakly bound van der Waals complex between the chaperon M and ClO. Reaction (5) produces (at least partially) stabilized ClOOCl*, since M carries away energy as it leaves.

$$ClO + M \Leftrightarrow ClO{\cdot}M \qquad (4,-4)$$

$$ClO + ClO{\cdot}M \rightarrow ClOOCl^{*} + M \qquad (5)$$

Depending on the energy distributions of the excited ClOOCl* and ClOOCl**, other reaction pathways may be accessible, such as

$$ClOOCl^{*} \rightarrow Cl + ClOO \qquad (6)$$

The purpose of this study is to determine the importance of the chaperon mechanism in the ClO + ClO + M reaction for M = N_2 and to determine its effect on subsequent reactions, such as Reaction (6).

Optimized geometries and frequencies for the stationary points involved in reactions (2,-2), (4,-4), and (5) are calculated at the B3LYP/6-311+G(3df) level of theory, and the energies are

further refined at the G3(MP2) level. Based on the theoretical results and some experimental values for structures and reaction barriers, we constructed analytical Cl_2O_2 and $Cl_2O_2N_2$ potential energy surfaces (PESs) for use in classical trajectory calculations using VENUS96.[3] The analytical PESs are expressed in terms of stretches, bends, torsions, non-diagonal stretch-stretch and stretch-bend interactions, and electrostatic attraction. Switching function parameters (to account for attenuation of force constants as bonds are broken) are determined from the theoretical calculations. The structures and vibrational frequencies calculated from the PESs are in very good agreement with the calculated and experimental properties of the stationary points.

Quasi-classical trajectory calculations performed using 10^5 trajectories for reactions (2) and (5) give rate constants of 2.91×10^{-12} and 2.4×10^{-12} cm^3 $molecule^{-1}$ s^{-1} at 300 K, respectively. The first of these is in reasonable agreement with the experimental[4] high pressure limit of Reaction (2); no experimental value is known for the second. The nascent energy distributions are obtained for the excited ClOOCl molecules produced according to the two mechanisms. We intend to use these distribution functions to carry out RRKM/master equation calculations to predict branching ratios, pressure dependence, etc. for the entire reaction system, including subsequent reactions like Reaction (6). These calculations are currently in progress.

References

1. L. T. Molina and L. J. Molina, *J. Phys. Chem.* 91, 443 (1987).
2. R. A. Cox and G. D. Hayman, *Nature* 332, 796 (1988).
3. W. L. Hase, R. J. Duchovic, X. Hu, A. Komornicki, K. F. Lim, D.-H. Lu, G. H. Peslherbe, K. N. Swamy, S. R. V. Linde, A. Varandas, H. Wang, and R. J. Wolf, *Quantum Chem. Program Exchange Bull.* **16** (4), 43 (1996).
4. (a) R. Atkinson, D. L. Baulch, R. A. Cox, J. Crowley, R. F. Hampson, M. E. Jenkin, J. A. Kerr, M. J. Rossi, and J. Troe, (IUPAC Subcommittee for Gas Kinetic Data Evaluation for Atmospheric Chemistry, Cambridge, 2002); (b) S. P. Sander, R. R. Friedl, A. R. Ravishankara, D. M. Golden, C. E. Kolb, M. J. Kurylo, R. E. Huie, V. L. Orkin, M. J. Molina, G. K. Moortgat, and B. J.Finlayson-Pitts, 2003.

Figure 1: PES of HN_3/TiO_2 system

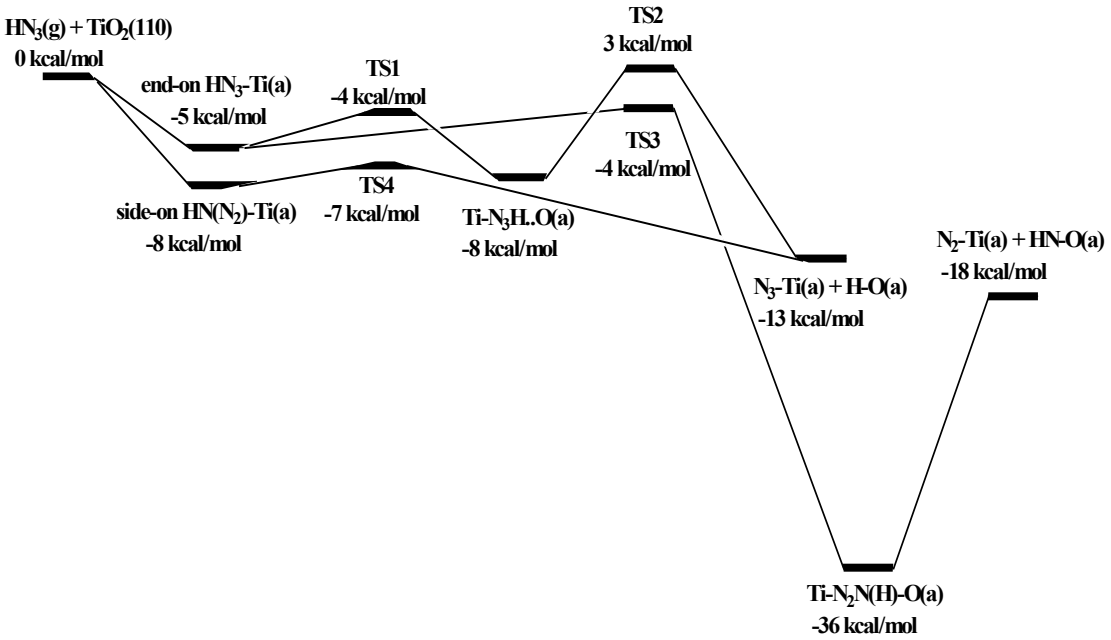

Figure 2: PES of $In(CH_3)_3/TiO_2$ system

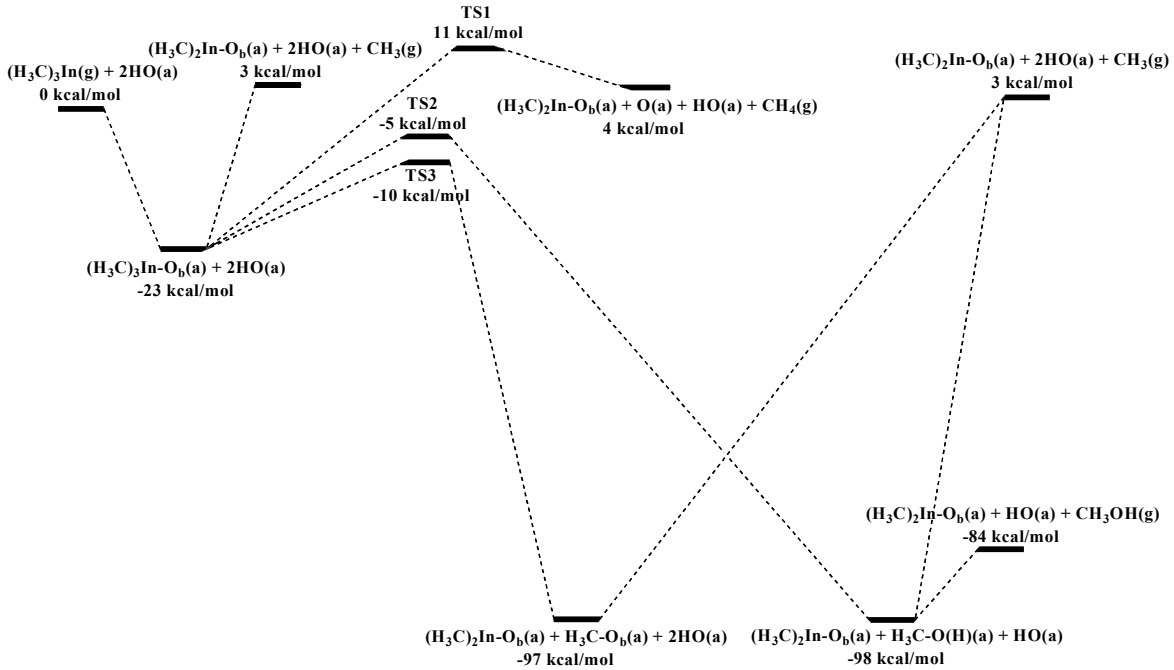

C7. Application of Automatic Reaction Model Generation to Chlorine-Initiated Neopentane Oxidation

***Sarah V. Petway*[a], *William H. Green*[b]**

[a]Massachusetts Institute of Technology, 77 Massachusetts Ave., Room 66-264, Cambridge, MA 02139, E-mail: petway@mit.edu
[b]Massachusetts Institute of Technology, 77 Massachusetts Ave., Room 66-270, Cambridge, MA 02139, E-mail: whgreen@mit.edu

A major challenge for the kinetics community is to develop methods for accurately predicting chemical kinetics a priori – this requires efficient construction of detailed models – as well as tools for comparing these models' predictions with experimental data, considering both the uncertainties in the data and all the uncertainties in the models. Ideally, one would be able to identify which rate constants or other parameters in the model are contributing the most to the uncertainties in the model predictions, and then to reduce the error bars on those key parameters. Here the MIT Reaction Mechanism Generator (RMG) developed by Jing Song was used to automatically generate a model for the chlorine-initiated oxidation of neopentane using initial reaction conditions described in the experimental investigation by DeSain, Klippenstein, and Taatjes [1]. Predicted concentration profiles for OH and HO_2 were compared to the experimental results. The option to perform first-order sensitivity analysis was implemented in RMG using DASPK 3.0, and a function to automatically generate approximate error bars on model predictions based on first-order sensitivity coefficients and uncertainties in rate and thermodynamic parameters was incorporated. The products of the normalized sensitivity coefficients and uncertainties in the estimated rate constants (expressed as ln(k)) were used to identify reactions that contribute most to the uncertainties in the predicted HO_2 and OH concentration profiles. The isomerization of the neopentylperoxy radical to the hydroperoxyneopentyl radical and the addition of oxygen to the hydroperoxyneopentyl radical contribute significantly to the uncertainty in both OH and HO_2 predictions because of the high sensitivities to these reactions. OH production is most sensitive to the initial hydrogen abstraction reaction of neopentane with a chlorine atom, while HO_2 production is sensitive to the addition of oxygen to the neopentyl radical.

References:

1. J. D. DeSain, S. J. Klippenstein, and C. A. Taatjes, *Phys. Chem. Chem. Phys.* 5, 1584-1592 (2003).

C8. OH-Initiated Oxidation of DMS and DMSO: Thermodynamic and Kinetic Theoretical Study

***Núria González-García*,[a] *Àngels González-Lafont*[b] *and José Mª Lluch*[c]**

Chemistry Department, Universitat Autònoma de Barcelona
08193 Cerdanyola del Vallès, Barcelona, SPAIN
[a] E-mail: nuria@qf.uab.es
[b] E-mail: Angels.Gonzalez@uab.es
[c] E-mail: JoseMaria.Lluch@uab.es

Dimethyl sulfide (DMS) atmospheric oxidation can have a notable climate impact since DMS oxidation products may contribute to aerosol formation and growth in the marine environment. [1,2] These aerosols influence the earth-atmosphere radiation budget both directly, through reflection from the aerosols of the incoming solar radiation, and indirectly, by modifying the formation processes of clouds and their albedo.
The main products containing sulfur of the OH-initiated oxidation of DMS are: dimethyl sulfoxide (DMSO), dimethylsulphone ($DMSO_2$), methanesulphonic acid (MSA), methanesulphinic acid (MSIA) and methane sulphonyl peroxynitrate (MSPN). [3-5] DMSO is a particulary stable product that is also obtained from the oxidation of the DMS by phototropic bacteria.[6] The global oxidation scheme for DMS is depicted in Figure1.

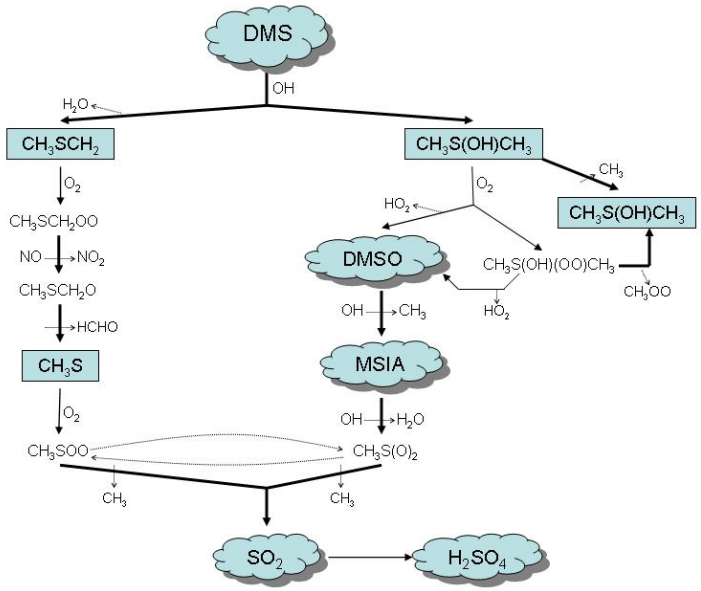

Figure 1: Global degradation scheme for DMS in the atmosphere (the studied routes are indicated with thicker lines)

The OH-initiated oxidation of DMS can proceed via two main different channels (the third one is negligible) that according to our results bifurcate at the dipole-dipole complex formed in the entrance channel.[7] In the absence of oxygen, the adduct (DMS-OH) is stabilized due to the high barrier for the elimination process that follows next. On the other hand, the H-abstraction takes place via a saddle point structure. The theoretical results agree quite well with the

branching ratios experimentally assigned: 0.8±0.26 and <0.07 at 298K for the formation of CH_3SCH_2 and CH_3SOH, respectively.
A wide set of electronic structure methods and basis sets were tested and we concluded that the choice of the most adequate electronic structure level is a very delicate matter that has to be considered with great caution. Our best estimation of the energetics was obtained at the MCG3/3//MPW1K/MG3S level.[8,9]
A kinetic study under the Variational Transition-State Theory formalism is now in progress in our lab.
Continuing with the main degradation routes of DMS, we performed a similar study on the DMSO plus OH reaction. Some experimental works have been published which discuss about the main channel of this reaction.

$$CH_3S(O)CH_3 + OH \rightarrow CH_3S(O)(OH)CH_3 \rightarrow CH_3S(O)OH + CH_3$$
$$CH_3S(O)CH_3 + OH \rightarrow CH_3S(O)CH_2 + H_2O$$
$$CH_3S(O)CH_3 + OH \rightarrow CH_3SO + CH_3OH$$

Our theoretical study [10] confirms that the main channel is the addition-elimination one, which implies the formation of MSIA. A Variational Transition-State Theory study has been performed and our results agree quite well with the rate constants published for this reaction in the most recent work: $(9\pm2)\times10^{-11}$ cm^3 $molec^{-1}$ s^{-1} at room temperature.[11]
Our aim is to continue working on these interesting reactions to achieve a better understanding of DMS degradation in the atmosphere.

REFERENCES

1. R. J. Charlson, J. E. Lovelock and M. O. Andreae, *Nature 326*, 655, **1987**
2. (a) F. Yin , D. Grosjean and J. H. Seinfeld, *J. Atmos. Chem. 11*, 309, **1990**; (b) F. Yin , D. Grosjean and J. H. Seinfeld, *J. Atmos. Chem. 11*, 365, **1990**
3. I. Barnes and K. H. Becker and I. Patroescu, *Atmos. Environ. 30*, 1805, **1996**
4. S. Sorensen and H. Falbe-Hansen and M. Mangoni and J. Hjorth and N. R. Jensen, *J. Atmos. Chem. 24*, 299, **1996**
5. C. Arsene and I. Barnes and K. H. Becker, *Phys. Chem. Chem. Phys. 1*, 5463, **1999**
6. P.T. Visscher and H. Gemerden, FEMS *Microbiol. Lett. 81*, 247, **1991**
7. N. González-García, À. González-Lafont and J. M. Lluch, *J. Comput. Chem. 26*, 569, **2005**
8. B. J. Lynch, P.L. Fast, M. Harris and D.G. Truhlar, *J. Phys. Chem. A 104*, 4812, **2000**
9. B. J. Lynch and D.G. Truhlar, *J. Phys. Chem. A 107*, 3898, **2003**
10. N. González- García, À. González-Lafont and J. M. Lluch, *submitted*
11. A. Kukui, D. Borissenko, G. Laverdet and G. Le Bras, *J. Phys. Chem. A 107*, 5732, **2003**

C9. Laboratory Study of Acetone Photolysis Under Tropospheric Conditions

***Carissa D. Howard*[1], *J. Michael Nicovich*[1], *Paul H. Wine*[1, 2]**

[1] School of Earth & Atmospheric Sciences, Georgia Institute of Technology,
311 Ferst Dr. NW, Atlanta, GA 30332-0340
[2] School of Chemistry & Biochemistry, Georgia Institute of Technology,
770 State St. NW, Atlanta, GA 30332-0400
Email: choward@eas.gatech.edu, mike.nicovich@chemistry.gatech.edu,
paul.wine@chemistry.gatech.edu

Acetone, $(CH_3)_2CO$, is a ubiquitous atmospheric species and is believed to be the most abundant oxygenated hydrocarbon in the atmosphere [1]. The major atmospheric sinks for acetone are the reaction with the hydroxyl radical (OH) in the lower troposphere and photo-dissociation in the upper troposphere. Photolysis of acetone is thought to be an important source of HO_x radicals in the upper troposphere [2]. In order to make an accurate assessment of the impact of acetone photolysis on HO_x radical production in the upper troposphere, absorption cross sections and photo-dissociation quantum yields as a function of wavelength, temperature, and pressure over the range of tropospheric conditions must be known quantitatively. A seemingly accurate set of acetone absorption cross sections as a function of wavelength and temperature have been reported [3]. However, the quantum yields reported in the most recent studies [3,4] are in poor agreement, resulting in a large uncertainty in the HO_x source strength from acetone photolysis. This uncertainty has provided motivation for us to carry out a detailed laboratory investigation of the photo-dissociation of acetone in air bath gas with the goal of quantitatively determining the needed quantum yields over the complete range of conditions relevant for modeling tropospheric chemistry.

Our study of acetone photochemistry employs a method that involves tunable dye laser photolysis in a high-pressure, temperature-controlled flow cell coupled to a detection system that utilizes chemical ionization mass spectrometry (CIMS). The range of conditions being investigated are $\lambda = 295 - 330$ nm, $T = 220 - 320$ K, and $P = 0.2 - 1.0$ atm. Our experimental approach is similar to that used by Molina and coworkers to measure the radical quantum yields from the photo-dissociation of O_3, Cl_2O, and H_2CO [5], and takes advantage of the sensitivity of the CIMS method developed by Huey and coworkers for detecting $CH_3C(O)OONO_2$ (PAN) [6]. A photolysis mixture containing acetone, CO, NO_2, and air is irradiated using a Nd:YAG laser pumped tunable dye laser. A fraction of the excited acetone molecules dissociate and produce CH_3CO, which is rapidly converted to $CH_3C(O)OO$ with a known high yield [7,8] by reaction with O_2. Subsequent reaction of $CH_3C(O)OO$ with NO_2 quantitatively converts this radical product to $CH_3C(O)OONO_2$ (PAN), which is stable at $T < 320$ K, but thermally dissociates at higher temperature. Before entering the CIMS detector the PAN molecules are passed through a heated cell with $T \sim 400$ K to convert the molecules back to $CH_3C(O)OO$ radicals, which are converted to acetate ($CH_3C(O)O^-$, mass = 59 amu) using I^- as the reagent ion. The ion signals at mass 59 and several other masses where acetate cluster ions form can be related to the $CH_3C(O)OO$ concentration using suitable calibration techniques that will be described. Only

room temperature experiments have been carried out to date. Pressure dependent quantum yield data at 298 K will be presented and compared with literature values.

References:

1. See for example, H. Singh, Y. Chen, A. Tabazadeh, Y. Fukui, I. Bey, R. Yantosca, D. Jacob, F. Arnold, K. Wohlfrom, E. Atlas, F. Flocke, D. Blake, N. Blake, B. Heikes, J. Snow, R. Talbot, G. Gregory, G. Sachse, S. Vay, and Y. Kondo, *J. Geophys. Res.*105, 3795-3805 (2000).

2. See for example, L. Jaegle, D.J. Jacob, W.H. Brune, and P.O. Wennberg, *Atmos. Environ.* 35, 469-489 (2001).

3. T. Gierczak, J.B. Burkholder, S. Bauerle, and A.R. Ravishankara, *Chem. Phys*. 231, 229-244 (1998).

4. M.A. Blitz, D.E. Heard, M.J. Pilling, S.R. Arnold, and M.P. Chipperfield, *Geophys. Res. Lett.* 31 (6), Art. no. L06111 (2004); Correction: *Geophys. Res. Lett.* 31 (9), Art. no. L09104 (2004).

5. See for example, G.D. Smith, L.T. Molina, and M.J. Molina, *J. Phys. Chem. A* 106, 1233-1240 (2002).

6. D.L. Slusher, L.G. Huey, D.J. Tanner, F.M. Flocke, and J.M. Roberts, *J. Geophys. Res.* 109 (D19), Art. no. D19315 (2004).

7. G.S. Tyndall, J.J. Orlando, T.J. Wallington, and M.D. Hurley, *Int. J. Chem. Kinet.* 29, 655-663 (1997).

8. M.A. Blitz, D.E. Heard, and M.J. Pilling, *Chem. Phys. Lett.* 365, 374-379 (2002).

C10. Ketone Photolysis Followed by the Reaction of RCO with O_2 as a Source of OH for Kinetic Studies of OH + ketone Reactions

M. T. Baeza Romero, M. A. Blitz, D. E. Heard, M. J. Pilling, B. Price*, P. W. Seakins

Dept of Chemistry, University of Leeds, LS2 9JT.
Email: B.Price: chm9bsjp@leeds.ac.uk
M. Baeza Romero: chmmtbr@leeds.ac.uk

Ketones play a key role in the atmosphere. They are primary and secondary pollutants, being intermediates in the oxidation of many VOC's and being emitted by biogenic (e.g. plant emissions) and anthropogenic sources (e.g. traffic pollution) [1]. Moreover, their photolysis is a source of free radicals and they can also interact with nitrogen oxides to produce photochemical smog.

The two key removal process for ketones in the atmosphere are by reaction with OH or by solar photolysis, with differing implications for radical and ozone formation [2],[3]. The magnitude and temperature dependence of the OH rate coefficients are required to determine the fraction of ketones removed by each process throughout the atmosphere. Previous studies of the reaction of OH with acetone [5] demonstrated complex temperature dependence and raised the possibility of multiple removal mechanisms.

Ketones photolysis at low pressure in the presence of oxygen and in the absence of NO has been shown to be a source of OH [2], [6], [7].

E.g. for acetone

$$CH_3COCH_3 \xrightarrow{h\nu} CH_3CO + CH_3$$
$$CH_3CO + O_2 \longrightarrow OH + products$$

With sufficient oxygen the timescale for OH production can be made very short compared to reaction of OH with the ketone, potentially making ketone/ O_2 mixtures a convenient source of OH.

a)

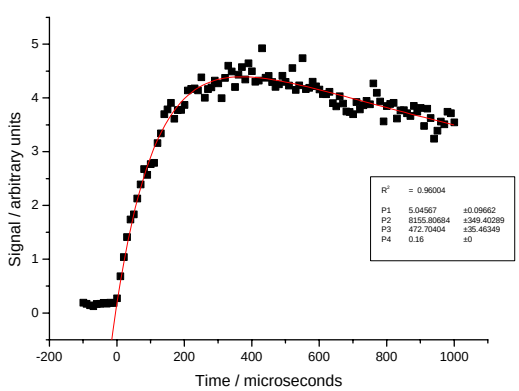

b)

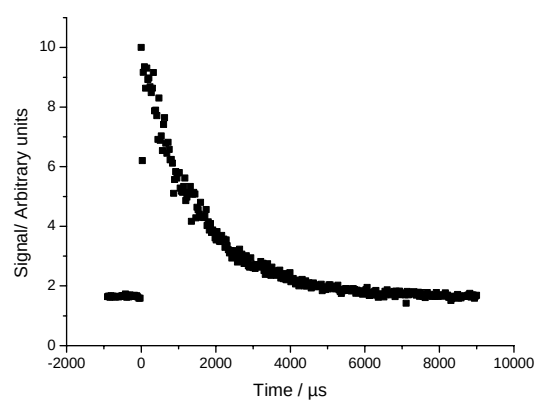

Figure 1: Typical Data obtained for MEK showing (a) OH production arising from MEK photolysis in an O_2/He mixture, and (b) the decay of OH due to reaction with MEK.

In this work, the photolysis of MEK (2-butanone) and DEK (3-pentanone) in the presence of excess oxygen has been used as an OH source to study the OH reaction with these two ketones.

The reaction of OH with the ketones was studied for pressures from 20-100 Torr at temperatures in the range 203-298 K providing good agreement with previous results [3], [4]. There was no observable pressure dependence in the range studied for either ketone at all temperatures.

The Arrhenius expression gave a rate coefficient for k_{MEK}= (1.13±0.25)x10^{-12}exp(-(46±61)/T) $cm^3 molecule^{-1} s^{-1}$ but the DEK presented a slight curvature in the Arrhenius plot [5].

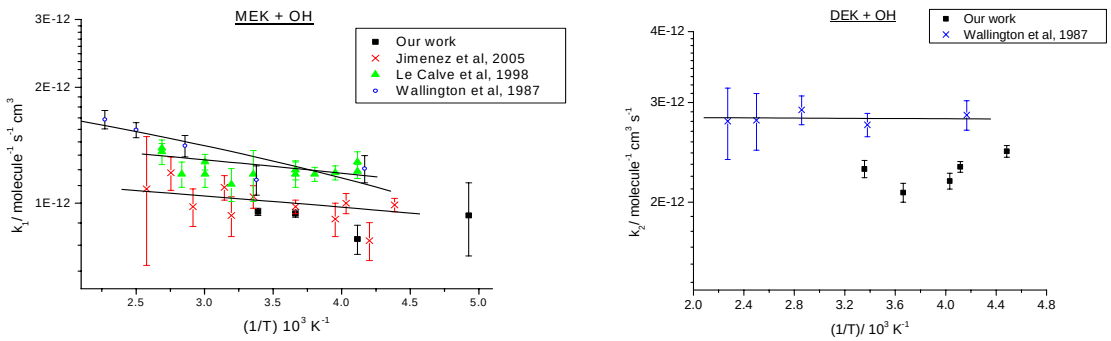

Figure 2: The Temperature dependence of the reaction of a) MEK with OH and b) DEK with OH.

The advantages and disadvantages of using ketone photolysis as an OH source have been studied against previous methods of OH generation (e.g. photolysis of precursors) to evaluate the possibility of using this novel approach as a widespread source for studying OH chemistry with ketones.

Moreover, the atmospheric relevance of these reactions has been studied for conditions present in different layers of the atmosphere.

References:

[1]National Atmospheric Emissions Inventory, Appendix 6: NMVOC emissions, 2000.

[2]M. A. Blitz *, D. E. Heard, M. J. Pilling. OH formation from CH_3CO+O_2: a convenient experimental marker for the acetyl radical. Chemical Physics Letters 365 (2002) 374–379.

[3]E. Jiménez, B. Ballesteros, E. Martinez, J. Albaladejo. Tropospheric reaction of OH with selected linear ketones: Kinetic studies between 228 and 405 K. Environ. Sci. Technol. 39 (2005) 814-820

[4]S. Le Calve, D. Hitier, G. Le Bras, A. Mellouki. "Kinetic Studies of OH reactions with a set of ketones." J. Phys. Chem. A 102 (1998) 4579-4584.

[5]M. Wollenhaupt, S. A. Carl, A. Horowitz, J.N. Crowley. "Rate Co-efficients for Reaction of OH with Acetone between 202K and 395K." J. Phys. Chem. A 104 (2000) 2695-2705.

[6] Photolysis of methylethyl, diethyl and methylvinyl ketones and their role in the atmospheric HOx budget. M. T. B. Romero, M. A. Blitz, D. E. Heard, M. J. Pilling, B. Price, P. W. Seakins* and L. Wang

[7]Is the photolysis of alkylketones a method to study their OH reactions? M. T. B. Romero*, M. A. Blitz, D. E. Heard, M. J. Pilling, B. Price, P. W. Seakins. *In publication*

C11. Chemical Kinetics of C_4 Alkanes Using New Evaluated Data

***Crina Heghes*[a], *Volker Karbach*[b], *Jürgen Warnatz*[c]**

Interdisciplinary Center of Scientific Computing, Im Neuenheimer Feld 368, IWR, 69120 Heidelberg, Germany, [a]E-mail: cheghes@iwr.uni-heidelberg.de,
[b]E-mail: karbach@iwr.uni-heidelberg.de, [c]E-mail: warnatz@iwr.uni-heidelberg.de

Combustion is a technologically important process so that its detailed description is desirable. Development and modelling of detailed chemical elementary reaction schemes is vital in understanding the nature of combustion processes. For obtaining useful information from numerical simulations, the kinetic and thermodynamic properties of the involved reactions and species must be valid.

In this work a new mechanism was developed on the basis of a previously available mechanism [2] and includes the reactions of high temperature combustion of H_2, CO, CH_4, C_2H_6, C_3H_8 and C_4H_{10}. In this mechanism we have implemented the new kinetic parameters evaluated by CODATA [1] project.

The mechanism consists of 450 elementary reactions and 62 species. The approximate temperature range is from 900 to 2500 K. For each development step of the mechanism, for each fuel considered, premixed laminar flames have been calculated, as well as ignition delay times, and compared with experiments for the largest possible condition range (initial temperature, pressure, equivalence ratio). Calculations of flame velocities and ignition delay times are performed to test the validity of the developed mechanism. Measurements of the ignition delay times are made behind reflected shock waves by observing the time delay in the onset of emission from excited hydroxyl radicals.

Sensitivity analysis has been performed in order to identify the rate limiting reactions and to understand the behaviour of the chemical system under different conditions. The rates of the elementary reactions in combustion processes differ greatly. Some reactions are so fast that the accuracy of the rate coefficients has a minor influence on the results of the mathematical modelling. For sensitive reactions, values for the rate coefficients have to be well known.

Furthermore, reaction flow analysis has been conducted to elucidate the important chemical pathways over a wide range of conditions. The integral flow analysis shows the percentage of the contributions of different reactions to the formation (or consumption) of the chemical species.

In the majority of reactions, the recommended Arrhenius parameters were used. Nevertheless, to obtain a better agreement between simulations and experiments, for a small number of reactions the recommended values were varied within the limits of experimental error of these reactions.

References:

1. D.L. Baulch, C.T. Bowman, C.J. Cobos, R.A. Cox, Th. Just, J.A. Kerr, M.J. Pilling, D. Stocker, J. Troe, W. Tsang, R.W. Walker, and J. Warnatz, Evaluated kinetic data for combustion modelling: Supplement II , 2004, to be published.
2. V. Karbach, PhD Thesis, Heidelberg University, 2005, in preparation.

C12. Reactions of O_2 with H_2, CH_4, H_2CO and C_2H_4

***Lawrence B. Harding*[a], *Stephen J. Klippenstein*[b], *Nanda K. Srinivasan*[a], *Meng-Chih Su*[c] *and Joe V. Michael*[a]**

[a]Chemistry Division, Argonne National Laboratory, Argonne, IL 60439
[b]Combustion Research Facility, Sandia National Laboratories, Livermore, CA 94551
[c]Department of Chemistry, Butler University, Indianapolis, IN 46208
E-mail: harding@anl.gov

Abstraction reactions involving ground state molecular oxygen with stable, closed shell molecules are thought to be important initiation reactions in some combustion systems. We report theoretical studies of the reactions,

$$H_2 + O_2 \rightarrow H + HO_2$$

$$CH_4 + O_2 \rightarrow CH_3 + HO_2$$

$$CH_2O + O_2 \rightarrow HCO + HO_2$$

$$C_2H_4 + O_2 \rightarrow C_2H_3 + HO_2$$

In each case we evaluate MP2 reaction paths and then CCSD(T) energies along these paths. The reactions paths determined in this way are used in transition state theory calculations of the rates for the reverse reactions and finally the reverse rates are transformed to forward rates using the equilibrium constants. Where possible the calculated rates are compared with recent experiments.

This work was supported by the U.S. Department of Energy, Office of Basic Energy Sciences, Division of Chemical Sciences, Geosciences, and Biosciences under Contract No. W-31-109-ENG-38.

C13. Theoretical studies on the kinetics and mechanisms of the O_3 + HO_2/HNO reactions

***Zhen-Feng Xu* and M. C. Lin**

Department of Chemistry, Emory University, Atlanta, GA 30322, USA
Email address: zhenfengxu@yahoo.com, chemmcl@emory.edu

The reactions of ozone with atmospheric species are of importance to the chemistry of the lower stratosphere and troposphere.[1] In this work, we study the kinetics and mechanisms for the reactions of ozone with HO_2 and HNO. The BH&HLYP/6-311++G(2df, 2p) level of theory has been employed to optimize the geometries of the reactants, products, intermediates and transition states. The reaction potential energy surfaces have been further improved with the G2M single-point energy calculations. The potential energy diagrams obtained at the G2M level of theory are shown in the following figures.

Interestingly, the results reveal that in both reactions the most favored paths take place by the OXH..O_3 (X = O and N) molecular complexes which fragment to give XO + HO_3 products. The direct transfer of an O atom from O_3 to HXO was found to be less competitive.

Based on the above predicted potential energy surfaces, the rate constants for these two reactions have been calculated by the Rice-Ramsperger-Kassel-Marcus theory and the variational transition state theory with the multiple reflections of the rate fluxes above the wells of the molecular complexes. The predicted results show that the rate constants for both reactions have a positive-temperature dependence with nearly no pressure effects. The predicted rate constants in the temperature range of 150 – 1000 K can be fitted into the expressions:

$$k(HO_2 + O_3) = 4.72 \times 10^{-29}\, T^{5.04} \exp(798.3/T)\ \ cm^3 molecule^{-1} s^{-1}$$
$$k(HNO + O_3) = 9.81 \times 10^{-29}\, T^{2.99} \exp(302.5/T)\ \ cm^3 molecule^{-1} s^{-1}$$

The former expression agrees reasonably with available experimental data[2-5] within the experimental temperature range of 200 – 400 K.

A. HO_2 + O_3

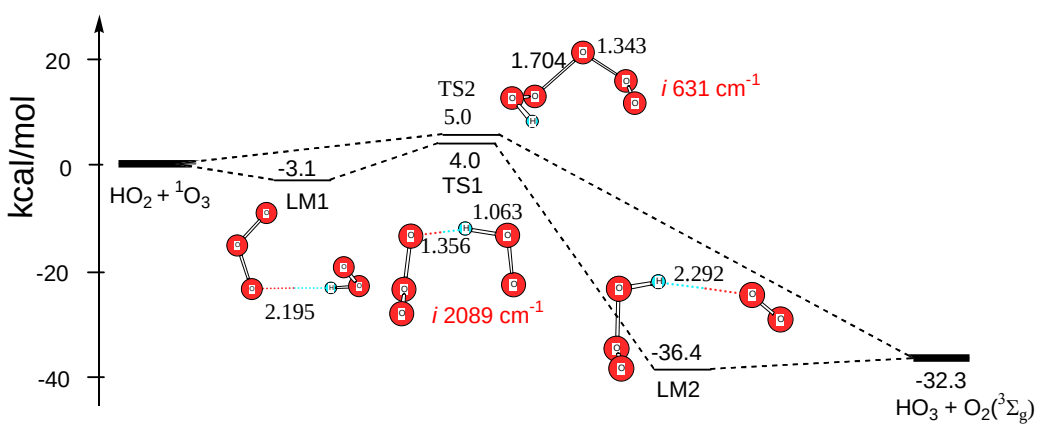

B. HNO + O_3

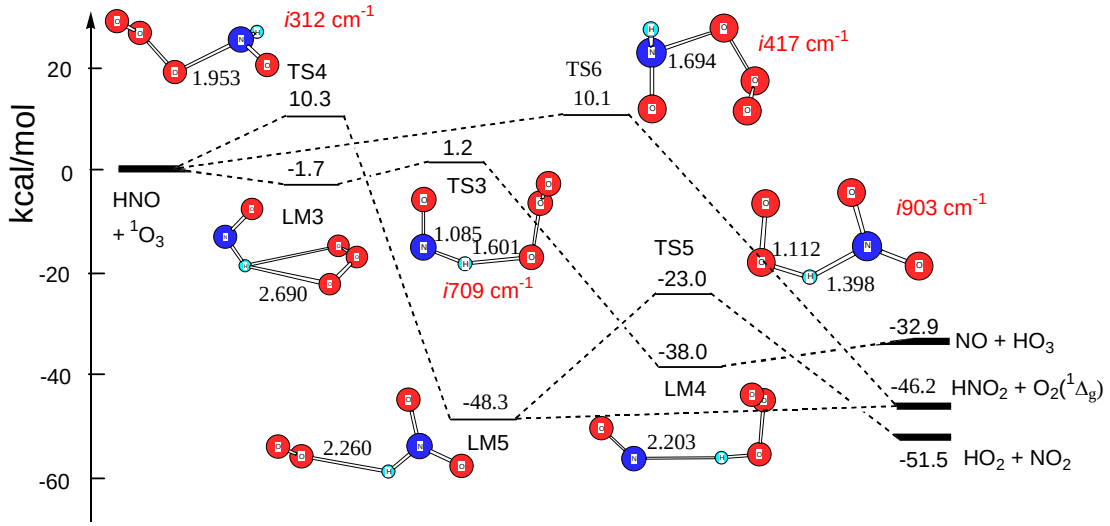

Reference:

[1] Whitten, R. C.; Borucki, W. J.; Capone, L. A.; Turco, R. P. **Effect of the reaction $HO_2 + O_3 \rightarrow OH + 2O_2$ on stratospheric ozone.** Nature (London, United Kingdom) (1978), 275(5680),

[2] Herndon, Scott C.; Villalta, Peter W.; Nelson, David D.; Jayne, John T.; Zahniser, Mark S. **Rate Constant Measurements for the Reaction of HO_2 with O_3 from 200 to 300 K Using a Turbulent Flow Reactor.** Journal of Physical Chemistry A (2001), 105(9), 1583-1591.

[3] Sinha, Amitabha; Lovejoy, Edward R.; Howard, Carleton J. **Kinetic study of the reaction of hydroperoxo (HO_2) with ozone.** Journal of Chemical Physics (1987), 87(4), 2122-8.

[4] Manzanares, E. R.; Suto, Masako; Lee, Long C.; Coffey, DeWitt, Jr. **Reaction rate constant of hydroperoxo + ozone (HO_2 + O_3) measured by detecting hydroperoxo from photofragment fluorescence.** Journal of Chemical Physics (1986), 85(9), 5027-34.

[5] Zahniser, Mark S.; Howard, Carleton J. **Kinetics of the reaction of hydroperoxo radical with ozone.** Journal of Chemical Physics (1980), 73(4), 1620-6.

C14. High Temperature Compact Mechanism Development for Large Alkanes: *n*-Hexadecane

Marcos Chaos[a], Andrei Kazakov[a], Frederick L. Dryer[a], Zhenwei Zhao[a], and Stephen P. Zeppieri[b]

[a] Mechanical and Aerospace Engineering Department, Princeton University, Princeton, NJ 08544
Email: mchaos@princeton.edu, andrei@princeton.edu, fldryer@princeton.edu, zzhao@princeton.edu
[b] United Technologies Research Center, East Hartford, CT 06108, USA
Email: ZeppieSP@utrc.utc.com

n-Hexadecane (cetane) is a reference fuel which, along with 2,2,4,4,6,8,8-heptamethylnonane, is used to estimate the cetane number rating of diesel fuels. Development of detailed chemical kinetics mechanisms for cetane will help to understand the performance and autoignition characteristics of diesel fuels and lead to the design of fuel surrogates to improve diesel engine efficiency and emissions. In addition, availability of such mechanisms may also be of relevance to the geologic community in predicting the stability of petroleum basins [1]. To date, however, very limited kinetic modeling [2-4] or experimental data exists for *n*-hexadecane oxidation [3, 4] and pyrolisis [5-9]. Furthermore, the size of the existing cetane mechanisms [2-4] makes their use prohibitive in numerical simulations of real combustion systems. Here, we extend a previously used approach [10, 11] to develop a compact mechanism for the pyrolisis and oxidation of *n*-hexadecane under high temperature conditions. The mechanism includes detailed treatment of the alkyl radicals formed, incorporating both internal hydrogen isomerization and β-scission reactions. In order to reduce the number of required species and simultaneously maintain the desired mechanistic detail, it was assumed that each of the alkyl radicals in the system exists in isomeric partial equilibrium above the C_4 level. As a result, only a single radical species is needed to represent all the isomers associated with it and the respective reaction channels associated with each isomer. A reduction of 54 species and 110 reactions was achieved using this approach for *n*-hexadecane. The resulting mechanism is validated against the available experimental data.

References

1. A. K. Burnham, H. R. Gregg, R. L. Ward, K. G. Knauss, S. A. Copenhaver, J. G. Reynolds, and R. Sanborn, *Geochim. Cosmochim. Ac.* 61, 3725-3737 (1997).
2. C. Chevalier, W. J. Pitz, J. Warnatz, C. K. Westbook, and H. Melenk, *Proc. Combust. Inst.* 24, 93-101 (1992).
3. A. Ristori, P. Dagaut, and M. Cathonnet, *Combust. Flame* 125, 1128-1137 (2001).
4. R. Fournet, F. Battin-Leclerc, P. A. Glaude, B. Judenherc, V. Warth, G. M. Côme, G. Scacchi, A. Ristori, G. Pengloan, P. Dagaut, and M. Cathonnet, *Int. J. Chem. Kinet.* 33, 574-586 (2001).
5. B. M. Fabuss, J. O. Smith, R. I. Lait, A. S. Borsanyi, and C. N. Satterfield, *Ind. Eng. Chem. Proc. Dev.* 1, 293- 299 (1962).

6. D. Depeyre, C. Flicoteaux, and C. Chardaire, *Ind. Eng. Chem. Proc. Dev.* 24, 1251-1258 (1985).
7. J. A. Fairburn, L. A. Behie, and B. W. Svrcek, *Fuel* 69, 1537-1545 (1990).
8. G. Wu, Y. Katsumura, C. Matsuura, K. Ishigure, and J. Kubo, *Ind. Eng. Chem. Res.* 35, 4747-4754 (1996).
9. E. Bartekova and M. Bajus, *Collect. Czech. Chem. Commun.* 62, 1057-1069 (1997).
10. T. J. Held, A. J. Marchese, and F. L. Dryer, F.L., *Combust. Sci. Tech.* 123, 107-146 (1997).
11. S. P. Zeppieri, S. D. Klotz, and F. L. Dryer, . *Combust. Inst.* 28, 1587-1595 (2000).

C15. Trajectory Study of Vibrational Deactivation in the OH(v) + NO_2 → $HONO_2$* → OH(v') + NO_2 Reaction System

Yong Liu [a]***, Lawrence L. Lohr*** [b]***, and John R. Barker*** [c]

[a] Department of Atmospheric, Oceanic, and Space Sciences, University of Michigan, Ann Arbor, MI 48109-2143

[b] Department of Chemistry, University of Michigan, Ann Arbor MI 48109-1055

[c] Department of Atmospheric, Oceanic, and Space Sciences, University of Michigan, Ann Arbor, MI 48109-2143

Quasiclassical trajectory calculations are used to investigate the dynamics of the OH(v) + NO_2 → $HONO_2$* → OH(v') + NO_2 recombination/dissociation reaction on an analytic potential energy surface (PES) that gives good agreement with the known structure and vibrational frequencies of nitric acid. The vibrational energy distribution of product OH(v') radicals is qualitatively similar to statistical distributions, but exhibits quantitative differences, probably at least partly due to the effects of slow IVR. Nonetheless, the trajectory results predict that vibrational deactivation of OH(v) via the $HONO_2$* transient complex is ~90% efficient, almost independent of the initial OH(v) vibrational level, in qualitative agreement with recent experiments. Tests are also carried out using the $HONO_2$ PES, but assuming the weaker bond strength found in HOONO (peroxynitrous acid). In this case, the predicted vibrational deactivation efficiencies are significantly lower and depend strongly on the initial vibrational state of OH(v), in disagreement with experiments. This result suggests that the HOONO PES may contain more inter-mode coupling than that of $HONO_2$. When the intermediate is strongly bound, the measured vibrational deactivation rate constant is a useful proxy for the recombination rate constant, but quantitative differences may still exist. Furthermore, the efficacy of the proxy method must be evaluated on a case-by-case basis.

C16. Fundamental Kinetic Database Utilizing Shock Tube Measurements

***David F. Davidson*, Ronald K. Hanson**

Mechanical Engineering Department, Stanford University, Stanford CA 94305-3032
E-Mail: dfd@stanford.edu, hanson@me.stanford.edu

We are continuing to generate a database of fundamental combustion-chemistry-related kinetic measurements based on shock tube measurements. This database includes ignition delay time data, species concentration time-history data, and reaction rate coefficient data measured and published primarily by the Mechanical Engineering Department of Stanford University.

The database includes ignition delay time measurements over a wide range of conditions (T, P, X_{fuel}, ϕ) for the following fuels: small fuels including hydrogen, methane, ethane and ethylene; normal alkanes including propane, n-butane, n-heptane and n-decane; branched alkanes including iso-butane, iso-pentane and iso-octane; cyclo-alkanes including JP-10; olefins including 1,3-butadiene; aromatics including toluene; and gasoline, ternary gasoline surrogates, and kerosenes/jet fuels. For the oxidation of selected fuels, the database also includes species concentration time history measurements of the following species: OH, CH, CH_3, CO_2 and CH_4. A new separate section of the database includes rate coefficient measurements of critical combustion reaction rates, including rate coefficient measurements of the reactions of OH with toluene, acetone, formaldehyde, and methyl radicals.

This database offers a variety of shock tube data taken under well-documented conditions in well-characterized shock tubes. Comparison of this work with that of other investigators permits the formation of reliable consensus values for many of these measurements and conditions.

Future work includes: ignition delay time measurements in other cyclo-alkanes and aromatics; increasing usable shock tube test times by incorporating real-time measurement of reflected shock temperature and pressures; species concentration time-histories of other species include benzyl, HCO, and formaldehyde; and documentation of previous rate coefficients measurements for the reactions of other species including reactions in the formaldehyde system.

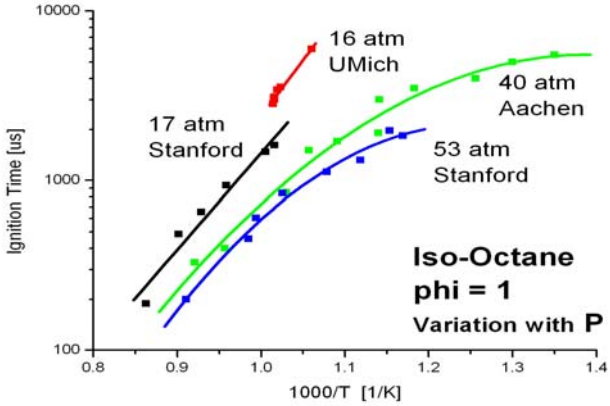

Fig. 1. Iso-octane ignition delay measurements: variation with pressure.

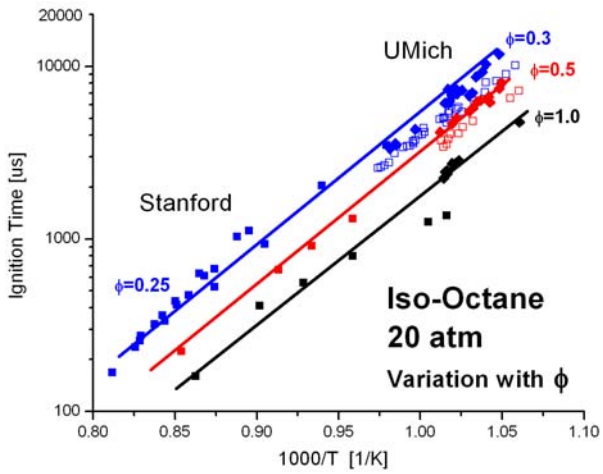

Fig. 2 Iso-octane ignition delay measurements: variation with equivalence ratio.

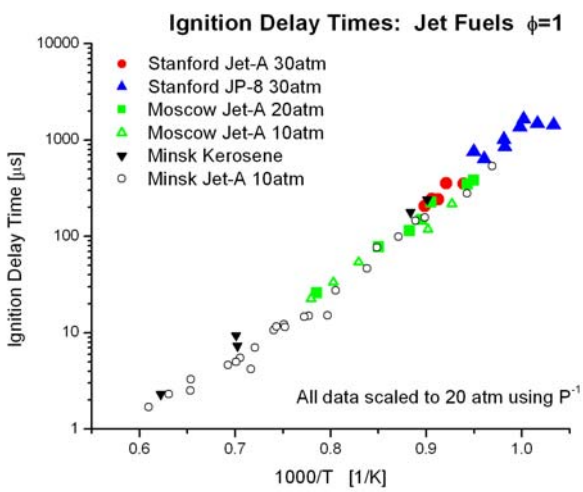

Fig. 3. Jet fuel ignition delay times: 20 atm

C17. State-to-State Rate Coefficients for Energy Transfer in H_2 as the Result of Collisions with H, He, or H_2

M. E. Mandy

Program in Chemistry, The University of Northern British Columbia, Prince George, British Columbia, CANADA V2N 4Z9 (mandy@unbc.ca)

An understanding of collisional energy transfer processes in molecular hydrogen is essential to the understanding of the relaxation of interstellar shocks and the associated quadrupole emission spectrum [1]. The interaction potentials are known to chemical accuracy for H_2 in collision with each of H [2], He [3], and H_2 [4]. Complete sets of cross sections and rate coefficients for state-to-state energy transfer and dissociation are being calculated with each of these potentials using the quasiclassical trajectory method. The validity of these results are benchmarked against the corresponding quantum calculations. The rate coefficients are parametrized with respect to temperature dependence and a web site is under development. Proposed Master Equation studies are also outlined.

References

1. Draine, B. T.; McKee, C. F. Ann. Rev. Astron. Astrophys. 1993, 31, 373.

2. Boothroyd, A. I.; Keogh, W. J.; Martin, P.G.; Peterson, M. J. J. Chem. Phys. 1991, 95, 4331.; 1996, 104, 7139

3. Boothroyd, A. I.; Martin, P. G.; Peterson, M. J. J. Chem. Phys. 2003, 119, 3187.

4. Boothroyd, A. I.; Martin, P. G.; Keogh, W. J.; Peterson, M. J. J. Chem. Phys. 2002, 116, 666.

C18. Self-recombination of the Hyponitrite Radical in Aqueous Solution

***Gregory A. Poskrebyshev*[1, *], *Sergei V. Lymar*[1]**

(1) Department of Chemistry, Brookhaven National Laboratory, 33 Lewis rd, bldg 555A, Upton, NY 11973, Fax: 631-344-5815,
* present address Oak Crest Institute of Science, 2275 E. Foothill Blvd., Pasadena, CA 91107, E-mail: poskr@yahoo.com

The hyponitrite radical ($HN_2O_2^{\bullet}$) may be produced by the combination of nitric oxide with nitroxyl (HNO) in a variety of NO-containing environments. This work presents a revision of the widely decay mechanism for this radical. The decay obeys second order kinetics throughout the *pH* range from 2 to 14, which suggests the reaction of self-recombination. In alkaline solutions, the reaction $2N_2O_2^{\bullet-} = N_2O_2^{2-} + 2NO^{\bullet}$ ($2k = 1.6 \times 10^{8}$ L mol^{-1} s^{-1}) is the main decay channel. In acid, the recombination branches into two channels: (a) $2HN_2O_2^{\bullet} = H_2N_2O_2 + 2NO^{\bullet}$ and (b) $2HN_2O_2^{\bullet} = HN_3O_3 + HNO$ with the branching ratio k_a/k_b=3 and the apparent rate constant $2k = 2k_a + 2k_b = 2.4\text{x}10^{9}$ L mol^{-1} s^{-1}. In both cases, the formation of $N_3O_3^{-}/HN_3O_3$ is observed and attributed mainly to the reactions $N_2O_2^{\bullet-} + NO^{\bullet}$ and $HN_2O_2^{\bullet} + NO^{\bullet}$. The values of rate constant for these reaction estimated in present work are found to be much higher than those reported previously. The HN_3O_3 intermediate exhibits $pK_a(HN_3O_3)$ of 3.4 and the rate constants for its decomposition into the final products ($NO_2^{\bullet} + N_2O$) are $k(N_3O_3^{-}) = 220$ s^{-1} and $k(HN_3O_3) = 4.8\text{x}10^{3}$ s^{-1}. The thermodynamics properties of HN_3O_3 are re-investigated using *ab-initio* calculations.

C19. Investigation Of Atmospheric Chemistry of Iodine Compounds

I.K. Larin[a], E.M. Trofimova[b], N.A. Messineva[c], A.I. Spassky[d], L.E. Turkin[e]

[a]Institute of Energy Problem of Chemical Physics, Russian Academy of Science,
119334 bld. 2, 35, Leninsky Avenue, Moscow, Russia
E-mail: iklarin@chph.ras.ru
[b]Institute of Energy Problem of Chemical Physics, Russian Academy of Science,
119334 bld. 2, 35, Leninsky Avenue, Moscow, Russia
E-mail: trofimova@chph.ras.ru
[c]Institute of Energy Problem of Chemical Physics, Russian Academy of Science,
119334 bld. 2, 35, Leninsky Avenue, Moscow, Russia
E-mail: messineva@chph.ras.ru
[d]Institute of Energy Problem of Chemical Physics, Russian Academy of Science,
119334 bld. 2, 35, Leninsky Avenue, Moscow, Russia
E-mail: spassky@chph.ras.ru
[e]Institute of Energy Problem of Chemical Physics,
Russian Academy of Science, 119334 bld. 2, 35, Leninsky Avenue, Moscow, Russia
E-mail: turkin@chph.ras.ru

The atmospheric reactions of iodine particles proceed mainly in the troposphere and through tropospheric chemistry influence on greenhouse effect and ozone layer.
Though stratospheric ozone depletion is connected with chlorine and bromine chemistry but some papers [1] point to the possible role of iodine compounds in these processes. Iodine particles are very reactive ones and ozone depletion in chain reactions with iodine compounds is even more considerable than in case of chlorine and bromine particles.

Main natural sources of atmospheric iodine particles are biogenic ocean processes producing methyl io $CH_3I + h\nu \rightarrow CH_3 + I$ ced in the photodissociation reaction

Then as $I + O_3 \rightarrow IO + O_2$ n with troposphere ozone

we have a very reactive particle – a radical IO which is mainly responsible for iodine atmospheric chemistry.

The complex study of homogeneous and heterogeneous chemical reactions of iodine compounds taking place in the Earth atmosphere were early carried out by the authors of the present thesis and described in [2]. Registration of iodine atoms by their resonance fluorescence signal due to enormous absorption cross section provides the high sensitivity of the technique and the possibility to carry out the studies at the low concentrations of IO radicals and atomic iodine to exclude the effect of secondary reactions of these compounds.

Reaction of ozone with iodine atoms have been studied at the temperature ranging from 231 K to 337 K. Another reaction of I

$$I + NO_2 + M \rightarrow INO_2 + M$$

was investigated for M= N_2, He, Ar, O_2.

Reactions of radical IO with chemical compounds

$$IO + A \rightarrow I + AO$$

where A= NO, CO, IO, H_2S, $(CH_3)_2S$, SO_2, O_3 were studied using a method based on measurement of steady-state concentration of I formed in the course of a chain chemical conversion, including the reaction studied as one of the steps. The steady-state concentration was determined from the resonance fluorescence signals of iodine atoms. The rate constant for A = NO was measured at temperature ranging from 293 K to 366 K.

A set of reactions of radicals IO with some chemical compounds without forming of iodine atoms was also investigated. In this case we converted radicals IO that had not been reacted into iodine atoms by the following fast reaction

$$IO + NO \rightarrow I + NO_2.$$

Registration of iodine atoms by the resonance fluorescence method permitted to have a high sensibility of the technique. We investigated reactions

$$IO + B \rightarrow products$$

for B= HCOOH, $CHCl_2CF_2Cl$, $CHFClCF_2Cl$, $CF_3CH_2OCHF_2$, CF_3OCH_2 and O_3 at 323 K. Trimolecular reaction

$$IO + NO_2 + O_2 \rightarrow INO_2 + O_2$$

was investigated using the mentioned above method at temperature ranging from 295 K to 343 K.

Measured rate constants of iodine particles reactions are in agreement with the results of other authors. Some of rate constants are originally obtained and are of importance for modeling atmosphere processes.

References:

[1] Solomon S., Garcia R.P., Ravinshankara F.R., J. Geophys. Res. 1994, v. 99, N D11110, p. 20491.
[2] S.N. Buben, I.K. Larin, E.M. Trofimova, A.I. Spassky, N.A. Messineva, L.E. Turkin, Kchimicheskaya Fisika (in Russian), 2002, v. 21, N 4, pp. 52-60.

C20. The Effect of Internal Energy of Molecules *Cscl* and *Rbj* on Dynamics of Their Collision-Induced Dissociation

V.M. Azriel, L.Yu. Rusin

Institute of Energy Problems of Chemical Physics RAS,

Leninskiì prospect 38, Bldg.2, Moscow 119334, Russia

E-mail: Vladimir.Azriel@sunchem.ru

Dynamics of bimolecular collision-induced dissociation (CID)

$$CsCl + RbJ \rightarrow Cs^{+} + Cl^{-} + Rb^{+} + J^{-} \qquad (1)$$

is investigated by quasiclassical trajectory technique described in details in [1]. Process represents special interest from the point of view of the mechanism of mutual transfer of energy, and also from the point of view of kinematics as a reaction that proceeds with formation of four particles from initial two. It is necessary to note rather high energy threshold of the reaction equal to the sum of threshold energies of disintegration of both molecules. In present calculations the collision energy was equal 13,0 eV.

Internal energies of reagents were chosen by Monte-Carlo technique for preset values of temperatures of sources of molecular beams in the assumption of equilibrium distributions on their states. Calculations were fulfilled for temperatures of sources of both beams equal 1000K, that corresponds to experimental conditions, for temperatures 300K and 3000K each source of a beam separately, and also for a case when temperatures of both sources are equal 1000K, but with the additive 0,172341 eV to relative energy of collision that corresponds to increase in temperature of a source on 2000K.

Cross section of CID decreases at downturn of any of temperatures of sources of beams of molecule-reagents and grows at their increase, and a little bit greater influence renders change of temperature of a source of a beam of molecules RbJ. Adequate change of relative energy of collision affects cross section of this channel in much smaller degree, than internal excitation of molecule-reagents.

As it was marked earlier in [2], at temperatures of sources of both molecular beams equal 1000K, angular distributions of products in the centre of mass system are characterized by scattering of ions Cs^{+} forward and ions Rb^{+} and Cl^{-} - backward. Thus scattering of ions J^{-} has no primary direction. Calculations show that the least sensitive to internal excitation of reagents is angular distribution of ions Cl^{-} which always scatter mainly in a back hemisphere. Ions Cs^{+} scatter forward, and this tendency becomes stronger with growth of internal energy of molecules RbJ. Simultaneously the backward scattering of ions Rb^{+} increase significantly. At the same time, growth of temperature of a source of a beam of molecules CsCl causes redistribution of angles of scattering of ions J^{-} which find out thus substantial growth of scattering in a back hemisphere. Corresponding angular distributions

for ions J^- at collision energy 13,0 eV and temperature of source of molecular beam of CsCl equal 1000K (a) and 3000K (b) are resulted on figure.

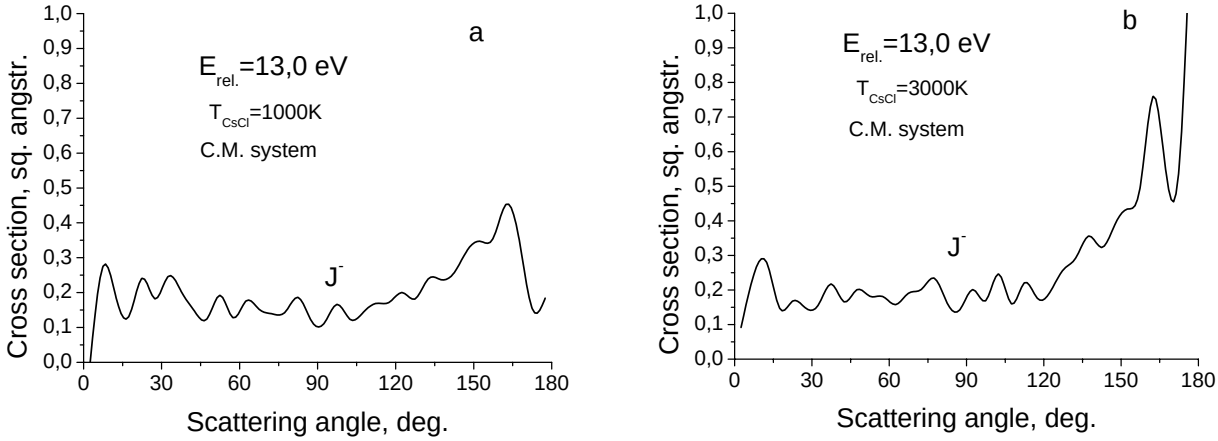

References:

1. V. M. Akimov, V. M. Azriel, L. Yu. Rusin, M. B. Sevryuk, *J. Chem. Soc. Faraday Trans*. 92, 1683 (1996).

2. V. M. Azriel, D. B. Kabanov, L. Yu. Rusin. Dynamics of collision-induced dissociation of two molecules with ionic bond. In: 24-th International Symposium on Rarefied Gas Dynamics (RGD24), Bari, Italy, 2004, *AIP Conference Proceedings* 762, 926 (2005).

C21. Shock Tube Pyrolysis of 1,2-Diiodobenzene – Kinetics of H Atom Production in High-Temperature Thermal Decomposition of *Ortho*-Benzyne

Chen Xu[a], Marina Braun-Unkhoff[a], Clemens Naumann[a], Peter Frank[a], Thomas Just[a], Xiaoqing You[b], and Hai Wang[b]

[a] DLR, German Aerospace Center, Institute of Combustion Technology, 70567 Stuttgart, Germany
[b] University of Southern California, Los Angeles, CA 90089, USA

It is generally accepted till now that the thermal decomposition of *ortho*-benzyne proceeds mainly through a concerted unimolecular process, leading to the formation of acetylene and diacetylene [1]

$$o\text{-}C_6H_4 \rightarrow C_2H_2 + C_4H_2 \qquad (\Delta H^0_{r,298} = 54 \text{ kcal/mol}). \qquad \text{(R1)}$$

If the above reaction is the sole pathway of benzyne decomposition, the H atom production can only be explained by the subsequent reactions of C-H fission in acetylene or diacetylene

$$C_nH_2 \rightarrow C_nH + H \quad (n = 2 \,\&\, 4) \qquad (\Delta H^0_{r,298} = 132 \text{ kcal/mol}) \qquad \text{(R2)}$$

or by the chemically activated reactions among acetylene and diacetylene,

$$C_mH_2 + C_nH_2 \rightarrow C_{m+n}H_3 + H \quad (m = n = 2,\ m = 2 \,\&\, n = 4;\ \text{or } m = n = 4) \qquad \text{(R3a)}$$
$$(\Delta H^0_{r,298} = \sim 66 \text{ kcal/mol})$$
$$C_{m+n}H_3 \rightarrow C_{m+n}H_2 + H \qquad (\Delta H^0_{r298} = \sim 40 \text{ kcal/mol}), \qquad \text{(R3b)}$$

Both types of reactions have been observed in shock tube pyrolysis of acetylene at very high temperatures (> 2200 K) [2,3]. In contrast, the direct H-atom production from *ortho*-benzyne is not currently understood. These reaction channels may include the mutual isomerization of *ortho*-, *meta*-, *para*-benzyne and the open ring C_6H_4 molecule (HC≡C–CH=CH–C≡CH), followed by thermally or chemically activated C-H fission of any of these C_6H_4 isomers.

In the present work, mechanism and kinetics of H atom production from the thermal decomposition of *ortho*-benzyne above 2000 K is investigated. The facile decomposition of 1,2-di-iodo-benzene allowed to produce ortho-benzyne in a direct step. Therefore, very low initial concentrations of 1,2-di-iodo-benzene are pyrolyzed behind reflected shock waves for $2000 < T/\text{K} < 2400$ at pressures around 2 atm. H atom production was monitored by the highly sensitive ARAS-technique. The simultaneous measurement of absorption of iodine atoms enables the *in situ* determination of the initial concentration of $o\text{-}C_6H_4$. Under these isolated conditions, production of H atoms was observed which increased rapidly with increasing post shock temperature.

Computationally we carried out quantum chemistry calculations at the CCSD(T)/6-31G(D)//B3LYP-6-31G(D) level of theory, followed by RRKM/master equation analysis of

thermal rate constants. The computation suggests that the lowest energy channels of H production appear to be the direct C-H fission from the three benzyne isomers (see, Figure 1). The C-H fission leads to the formation of cyclic C_6H_3 isomers, which are seen to lie lower in energy than the open-chain, C_6H_3 isomer. Thus, relative to the energy of *ortho*-benzene, the endothermicity of these H-production channels are 106 to 113 kcal/mol. These reaction enthalpies are notably smaller than the overall endothermicity of the competing channel, i.e., reactions (R1) and (R2) with $\Delta H_1 + \Delta H_2 = 186$ kcal/mol, but they are comparable with that of the chemically activated processes (R3a) with $\Delta H_1 + \Delta H_{3a} = \sim 110$ kcal/mol. The cyclic C_6H_3 radicals readily undergo ring opening. This is followed by H ejection from the resulting HC≡C–CH=C•–C≡CH radical to yield C_6H_2.

With the above understanding, thermal rate constants of channels relevant to *ortho*-benzyne decomposition and H atom production will be computed and compared with the shock tube data.

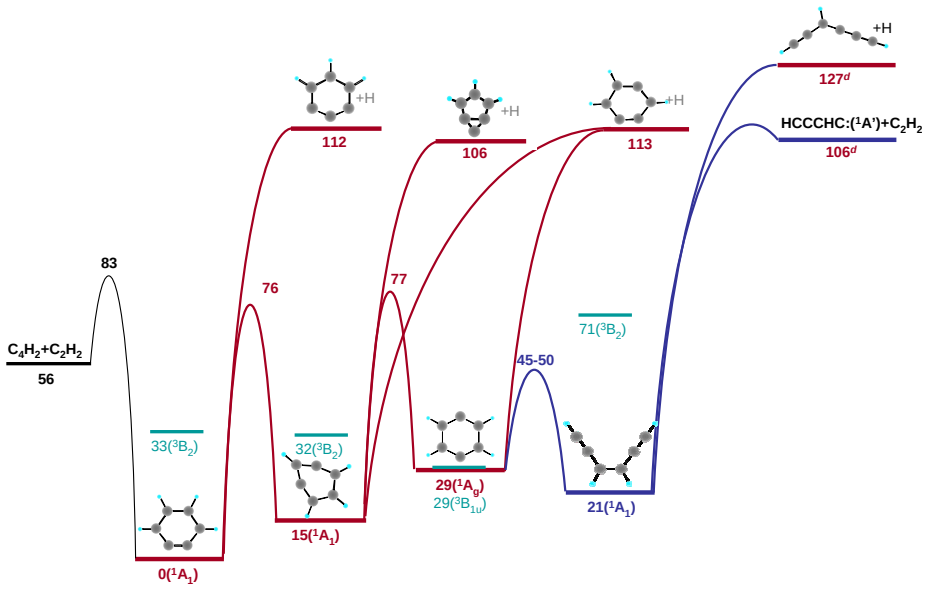

Figure 1. Potential energy for the unimolecular decomposition of *ortho*-benzyne, computed at the CCSD(T)/6-31G(D)//B3LYP-6-31G(D) level of theory. For comparison, the lowest lying triplet states are shown for the C_6H_4 isomers considered.

References

1. Wang, H., Laskin, A., Moriarty, A. and Frenklach, M., "On unimolecular decomposition of phenyl radical," *Proceedings of the Combustion Institute*, **28**, pp. 1545-1518 (2000).
2. Frank, P and Just, Th. "High temperature thermal decomposition of acetylene and diacetylene at low relative concentrations," *Combust. Flame* 38: 231-248 (1980).
3. Kiefer, J. H., Sighu, S. S., Kern, R. D., Xie, K., Chen, H., and Harding, L. B. "The homogeneous pyrolysis of acetylene .2. The high-temperature radical chain mechanism," *Combust. Sci. Technol.* 82: 101-130 1992.

C22. Complete Database of Chemical Bond Energies

Yu-Ran Luo

Marine Science, University of South Florida,
140 7th Av. South, St. Petersburg, FL 33701
E-mail: luo@marine.usf.edu

Chemical bond dissociation energies (enthalpies, BDEs) are fundamental to chemistry. There are about 100 chemical databases today. But, a complete BDE database has been a gap so far. We are establishing the BDE database. It includes:

- BDEs in diatomic molecules and ions
- BDEs in organic, biochemicals and non-metallic compounds, and their free radicals (C-, O-, N-, S-, Si-, Ge-, Sn-, Pb-, P-, As-X bonds)
- BDEs in inorganic compounds, ions, and the free radicals
- BDEs in organometallic compounds, ions, and the free radicals
- BDEs in clusters (neutrals and ions)
- BDEs in supramolecules
- BDEs in hydrogen-bonded species (neutrals and ions)
- BDEs in van der Waals complexes
- BDEs in surface-bonded species

The BDE data of 18,300 bonds of 102 elements from 5,000 publications have been collected:

Organics, biochemicals, non-metallics, radicals		bond #	Inorganics, organometallics, metallics, clusters, ions, supramolecules ,complexes		bond #	Total bond #
Ch. 3	C-H	1190	Ch. 11	H-,Li-,Na-,K-,Rb-,Cs-X	1186	4927
Ch. 4	C-C	690	Ch. 12	Be-,Mg-,Ca-,Sr-,Ba-,Ra-X	351	13415
Ch. 5	C-X	462	Ch. 13	Sc-,Y-,La-,Ac-X	788	18342
Ch. 6	O-X	1232	Ch. 14	Ti-,Zr-,Hf-X	302	
Ch. 7	N-X	668	Ch. 15	V-,Nb-,Ta-X	369	
Ch. 8	S-, Se-, Te-, Po-X	283	Ch. 16	Cr-,Mo-,W-X	884	
Ch. 9	Si-,Ge-,Sn-,Pb-X	289	Ch. 17	Mn-,Tc-,Re-X	284	
Ch. 10	P-,As-,Sb-,Bi-X	113	Ch. 18	Fe-,Ru-,Os-X	698	
		4927	Ch. 19	Co-,Rh-,Ir-X	676	
			Ch. 20	Ni-,Pd-,Pt-X	865	
			Ch. 21	Cu-,Ag-,Au-X	827	
			Ch. 22	Zn-,Cd-,Hg-X	153	
			Ch. 23	B-,Al-,Ga-,In-,Tl-X	514	
			Ch. 24	C-,Si-,Ge-,Sn-,Pb-X	1089	
			Ch. 25	N-,P-,As-,Sb-Bi-X	1265	
			Ch. 26	O-,S-,Se-,Te-, Po-X	1801	
			Ch. 27	F-,Cl-,Br-,I-,At-X	1235	
			Ch. 28	He-,Ne-,Ar-,Kr-,Xe-,Rn-X	128	
				102 elements	13415	

Using the following guide, the searching the BDE data becomes quick and easy.

A guide to search BDE data

C-H – Ch. *3*	**O-X** – Ch. *6*	**Si-, Ge-, Sn-, Pb-X** – Ch. *9*
C-C – Ch. *4*	**N-X** – Ch. *7*	**P-, As-, Sb-, Bi-X** – Ch. *10*
C-halogen – Ch. *5*	**S-, Se-, Te-, Po-X** – Ch. *8*	

The BDEs data of the following neutrals, radicals, ions and clusters are compiled.
The red numbers represent Chapters of these M-, M^+- and M^--X BDE data

H *11*																	**He** *28*
Li *11*	**Be** *12*											**B** *23*	**C** *24*	**N** *25*	**O** *26*	**F** *27*	**Ne** *28*
Na *11*	**Mg** *12*											**Al** *23*	**Si** *24*	**P** *25*	**S** *26*	**Cl** *27*	**Ar** *28*
K *11*	**Ca** *12*	**Sc** *13*	**Ti** *14*	**V** *15*	**Cr** *16*	**Mn** *17*	**Fe** *18*	**Co** *19*	**Ni** *20*	**Cu** *21*	**Zn** *22*	**Ga** *23*	**Ge** *24*	**As** *25*	**Se** *26*	**Br** *27*	**Kr** *28*
Rb *11*	**Sr** *12*	**Y** *13*	**Zr** *14*	**Nb** *15*	**Mo** *16*	**Tc** *17*	**Ru** *18*	**Rh** *19*	**Pd** *20*	**Ag** *21*	**Cd** *22*	**In** *23*	**Sn** *24*	**Sb** *25*	**Te** *26*	**I** *27*	**Xe** *28*
Cs *11*	**Ba** *12*	**La** *13*	**Hf** *14*	**Ta** *15*	**W** *16*	**Re** *17*	**Os** *18*	**Ir** *19*	**Pt** *20*	**Au** *21*	**Hg** *22*	**Tl** *23*	**Pb** *24*	**Bi** *25*	**Po** *26*	**At** *27*	**Rn** *28*
Fr *11*	**Ra** *12*	**Ac** *13*															

Note: red number, as *20,* shows the BDEs of Ni(Ni^+, Ni^-)-, Pd(Pd^+, Pd^-) and Pt(Pt^+, Pt^-)–X bonds are listed in Chapter 20.

The ***Sample:***

The broken bonds (**boldface** = dissociated atom or group)	BDEs (**boldface** = recommended data; references in parentheses)		Methods (references in parentheses)	References
	kcal/mol	kJ/mol		
Fe^+–CH	(1) 101±7	423±29	(1) Photodissoc.	(1) 1986HET/FRE
–CH_2	(1) 82±7 (2) 82.6±1.5 (3) **81.5±1**	343±29 346±6 **341±4**	(2) GIB MS (3) Review	(2) 1992SCH/ARM(b) (3) 1996ARM/KIC
–CH_3	(1) 65±5 (3) **54.7±1.2** (4) <69 (5) 69±5 (6) 57.1±2.3	272±21 **229±5** <289 289±21 239±10	(4) Ion reactions (5) Ion reactions (6) GIB MS	(4) 1979ALL/RID (5) 1984JAC/FRE(b) (6) 1989FIS/SCH